NASA TN D-637

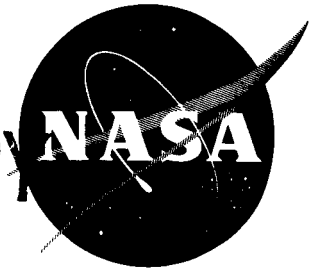

TECHNICAL NOTE

D-637

WIND-TUNNEL INVESTIGATION OF THE EFFECTS OF WING BODIES, FENCES, FLAPS, AND A FUSELAGE ADDITION ON THE WING BUFFET RESPONSE OF A TRANSONIC-TRANSPORT MODEL

By Elden S. Cornette

Langley Research Center
Langley Field, Va.

NATIONAL AERONAUTICS AND SPACE ADMINISTRATION

WASHINGTON

April 1961

NATIONAL AERONAUTICS AND SPACE ADMINISTRATION

TECHNICAL NOTE D-637

WIND-TUNNEL INVESTIGATION OF THE EFFECTS OF WING BODIES, FENCES, FLAPS, AND A FUSELAGE ADDITION ON THE WING BUFFET RESPONSE OF A TRANSONIC-TRANSPORT MODEL

By Elden S. Cornette

SUMMARY

The experimental wing buffet response of a transport-type airplane model with and without wing bodies, fences, flaps, and a fuselage addition has been investigated at Mach numbers from 0.20 to 1.03. The wing had NACA 64A-series airfoil sections inclined 5° to the free-stream direction. The quarter-chord line of the wing was swept back 45°, the aspect ratio was 7, the taper ratio was 0.3, and the thickness ratio varied from 0.115 at the root to 0.074 at the midsemispan and was constant from that station to the tip. The wing was twisted and cambered for a design lift coefficient of 0.3.

The results of the investigation indicated that a marked reduction of buffet intensity and a delay of buffet onset at transonic speeds were achieved by the addition to the wing of special bodies designed to reduce shock-induced separation. The further addition of wing fences and wing trailing-edge flaps deflected 30° increased the lift coefficients at which low-speed stall buffeting occurred. An addition to the fuselage near the upper forward portion produced no consistent change in the buffet characteristics.

INTRODUCTION

Recent wind-tunnel experiments (refs. 1, 2, and 3) indicate that considerable improvement in the aerodynamic efficiency of high-speed transport-type airplanes can be achieved by making certain additions to current configurations. References 1 and 2 show that a substantial reduction in drag, increase in drag-rise Mach number, and reduction and delay of pitch-up tendencies can be accomplished by adding special bodies to the upper surface of the wing and an addition to the upper portion of the fuselage. Such additions to current designs offer possibilities for substantial increases in maximum and cruise speeds without additional thrust.

The primary aerodynamic effect of the fuselage and wing additions is to reduce the strength of the shock waves and associated flow separation on the wing at lifting conditions. Since the primary external aerodynamic forces which excite wing buffeting are due to the random pressure fluctuations existing in regions of separated flow, it seemed reasonable to expect the fuselage and wing additions to reduce the wing-buffet response in the high-subsonic and transonic speed range. The objective of the present investigation, therefore, was to obtain experimental wing-buffet data on a transonic transport-type airplane model and to establish any buffet-alleviation properties of the wing bodies and the fuselage addition.

It has been found that wing-buffet data can be obtained simultaneously with ordinary force tests on a wind-tunnel model by the simple installation of a strain-gage bridge near the wing root. Reference 4 is an example of this type of wind-tunnel buffet testing. The root-mean-square value of the randomly fluctuating wing bending moment and the bending-moment power spectral density are considered to provide a satisfactory description of wing buffeting. The buffet data obtained in this investigation were recorded simultaneously with six-component force data which are reported in reference 3.

The configurations investigated included the clean model, which is similar to currently operating airplanes, with and without various combinations of wing bodies, fences, flaps, and a fuselage addition. The tests were conducted in the Langley 8-foot transonic pressure tunnel at Mach numbers from 0.20 to 1.03. The angle-of-attack range was from slightly below zero lift to 14° or to the maximum obtainable as dictated by model, balance, and support-system load limitations. The majority of the data were recorded at a tunnel stagnation pressure of 0.4 atmosphere.

SYMBOLS

a vertical distance from the center line of the basic fuselage to the center line of the fuselage addition, in.

b wing span, in.

c local wing chord parallel to free-stream direction, in.

$\bar{c}$ mean aerodynamic chord of wing, $\frac{2}{S}\int_0^{b/2} c^2 dy$, 7.08 in.

C_L lift coefficient, $\frac{\text{Lift}}{qS}$

g	structural damping coefficient
M	free-stream Mach number
p_t	free-stream total pressure, atm
q	free-stream dynamic pressure, $\frac{\rho V^2}{2}$, lb/sq ft
r	local radius of basic fuselage or wing body, in.
r_a	local radius of fuselage addition, in.
R	Reynolds number based on $\bar{c}$
S	wing planform area, 2.0 sq ft
t	local airfoil maximum thickness, in.
V	free-stream velocity, ft/sec
x	distance along center line from nose of fuselage or along wing-body center line from wing leading edge, in.
y	spanwise distance measured perpendicular from fuselage center line, in.
α	angle of attack of fuselage center line, deg
γ	aerodynamic damping ratio based on critical damping
ρ	free-stream density, slugs/cu ft
σ	root-mean-square wing bending moment due to buffeting (standard deviation from the mean), in-lb
σ_f	σ with response in rigid body modes electrically filtered out, in-lb
σ_{tc}	σ obtained from thermocouple mean-square meter, in-lb
σ_{tc}'	σ_{tc} with noise level tare (19 in-lb) subtracted out, in-lb
σ_i	σ obtained by integrating buffet response power spectrums, in-lb

Configuration components:

W	wing (6° dihedral, 2° incidence)
WB	wing bodies located at stations 1 0.33 semispan 2 0.57 semispan 3 0.80 semispan 4 wing tip f designates fences on wing bodies
WF	wing flaps extending to indicated semispan station (deflected 30°)
F	fuselage
FA	fuselage addition
VT	vertical tail
HT	horizontal tail (2° incidence)

APPARATUS AND TESTS

Tunnel

The investigation was conducted in the Langley 8-foot transonic pressure tunnel. This tunnel is a single-return type with a rectangular test section. The upper and lower walls are slotted longitudinally to allow continuous operation through the transonic speed range with negligible effects of choking and blockage. The entire test section is inclosed in a large pressure tank and, through the use of auxiliary compressors, the stagnation pressure can be controlled from 1/4 to to 2 atmospheres. During the tests, automatic temperature controls maintained a constant and uniform stagnation temperature of 123° F. The dewpoint was maintained near 0° F.

The local Mach number distribution throughout the test-section length occupied by the model was reasonably uniform. The maximum deviation from the average free-stream Mach number was of the order of 0.008 at the highest test Mach numbers and considerably less than this at the lower Mach numbers. Changes in free-stream stagnation pressure have essentially no effect on the Mach number distributions. Preliminary data indicate that the turbulence level in the test section is reasonably low.

Model Description

The airplane model used in this investigation was a transport which incorporated various configuration changes designed to promote greater efficiency of operation in the transonic speed range. The model was constructed for static force tests, and no attempt was made to scale it dynamically. A photograph of the model is shown in figure 1 and a three-view drawing is shown in figure 2. A detailed description of the model is also given in reference 3.

The basic fuselage had a fineness ratio of approximately 13. The rear portion of the fuselage was indented to provide improvements of the total area development in the region of the vertical and horizontal tails. The fuselage addition, which was concentrated on the upper, forward part of the fuselage, provided a desired fuselage camber as well as an improved area distribution. Cross sections and the longitudinal contour of the fuselage addition are shown in figure 3. The coordinates of the basic fuselage and fuselage addition are given in table I. The fuselage addition used in this paper is the same as the "modified" addition used in reference 3.

The wing was machined from a solid block of SAE 4130 steel and was heat treated to a Rockwell hardness of C34 to 36. It was twisted about the 50-percent-chord line and cambered to obtain a lift distribution which would provide good high-speed characteristics at a lift coefficient of about 0.3. The spanwise twist and thickness distributions are shown in figure 4. For the tests reported herein, the wing was mounted on the fuselage at an angle of incidence of 2° relative to the fuselage center line. That is, the angle of incidence of the chord line at any semispan station was 2° greater than the twist shown in the curve of figure 4. The dihedral angle was 6°.

The wing, as originally designed, had 40° of sweepback of the 0.25 chord line, an aspect ratio of 8, and a taper ratio of 0.3. The thickness varied linearly from 12 percent chord at the root to 8 percent chord at the 50-percent-semispan station with 8 percent chord from that station to the tip. NACA 64A-series airfoil sections, parallel to the free stream, were used across the entire wing span. During construction of the wing, experimental evidence from studies reported in reference 1 indicated that significant alleviation of the pitch up of sweptback wings provided by special bodies added to the wing considerably relaxed the limitation on wing sweep. For the present investigation, therefore, the sweep of the 0.25 chord line of the wing was increased to 45°. This increase in sweep was accomplished simply by rotating the 40° sweptback wing about the intersection of the 0.50 chord line and the fuselage center line until the 0.25 chord line was swept back 45°. The following dimensional characteristics evolved: an aspect ratio of approximately 7, a taper ratio of 0.3, a thickness

variation of from 11.5 percent chord at the root to approximately 7.5 percent chord at the midsemispan station with a thickness of 7.5 percent chord from that station to the tip. Other details of the wing are shown in figure 2 and presented in reference 3.

As a means of reducing the flow separation on the outer sections of the wing at lifting conditions, a series of bodies were added on the upper surface of the wing. The bodies were placed on the wing at 33-, 57-, and 80-percent-semispan stations as shown in figure 5 and were canted 3° with respect to the free-stream direction. The effect of another smaller body placed at each wing tip in a manner similar to the inboard bodies was also investigated. The coordinates of the bodies are given in table II. During a part of the investigation, chordwise wing fences were extended from the wing leading edge back along the forward portion of all the bodies except those at the wing tips. The fences had a maximum height of 0.25 inch and were faired tangent to the top of the wing bodies as shown in figure 5 where their contours are indicated. In the plan view, the fences were gradually turned slightly outboard near the leading edge so that their nose angle was 6° with reference to the plane of symmetry.

Trailing-edge flaps were tested on the model with wing bodies, fences, and fuselage addition at speeds up to a Mach number of 0.6. Two sets of flaps were used. One set covered the inboard span of the wing from 7.7 percent semispan to 33 percent semispan. The second set extended the region covered by the first set out to the 57-percent-semispan station. The flap chord was 25 percent of the local wing chord. The flap deflection angle, measured in a plane perpendicular to the trailing edge and with respect to the lower surface of the wing (fig. 6), was 30°.

An all-movable horizontal tail having NACA 65A006 airfoil sections oriented in the streamwise direction was mounted on the fuselage center line. The angle of incidence of the horizontal tail with respect to the fuselage center line was maintained at 2° for the investigation reported herein. The vertical tail, which also had NACA 65A006 airfoil sections oriented in the streamwise direction, was located slightly forward on the fuselage relative to the horizontal tail.

Transition strips were used on the model during the entire investigation to insure a turbulent boundary layer. One-tenth-inch-wide strips of No. 60 carborundum grains were applied around the nose of the fuselage 10 percent of the fuselage length back from the nose and along the 10-percent-chord line of the upper and lower surfaces of the wing, horizontal tail, and vertical tail.

The components which comprise each configuration are listed as follow:

Configuration	Components
1	W + F + VT + HT
2	W + F + FA + VT + HT
3	W + WB (1, 2, 3) + F + FA + VT + HT
4	W + WB (1f, 2f, 3f) + F + FA + VT + HT
5	W + WB (1f, 2f, 3f, 4) + F + FA + VT + HT
6	W + WB (1f, 2f, 3f) + WF (0.33 semispan) + F + FA + VT + HT
7	W + WB (1f, 2f, 3f) + WF (0.57 semispan) + F + FA + VT + HT

The weights of the various model components are given in table III.

Instrumentation

A block diagram of the instrumentation used to record the buffet data is shown in figure 7. The strain-gage bridge used to measure the wing buffet bending consisted of four active arms and was temperature compensated. The strain gages were mounted in shallow pockets machined in the upper and lower surfaces of the left wing panel near the root and were oriented with their sensitive axes adjacent and parallel to the 50-percent-chord line in order to measure bending about an axis approximately perpendicular to the 50-percent-chord line. (See fig. 8.) The strain-gage bridge was energized by a 3-kilocycle-per-second alternating voltage, and the output signal was the amplitude modulated carrier. The unbalance due to static load levels was not recorded in the data since the linear amplifier passed only that portion of the signal due to buffeting at frequencies from approximately 5 to 5,000 cps. The random buffet signal was recorded on magnetic tape using 45-second data samples, and the mean-square value of the bending moment was visually recorded from a thermocouple-type mean-square meter. A low-frequency oscillator and root-mean-square voltmeter were used to supply a known calibration signal to the tape recorder and thermocouple meter. A d-c millivolt meter was used in connection with static-load bending-moment calibration of the strain-gage bridge performed previous to the wind-tunnel tests. (See section on model calibrations and shake tests.)

Incorporated within the model was a six-component strain-gage balance used to obtain static lift coefficients and a strain-gage pendulum device used to measure the angle of attack of the fuselage center line. The static lift coefficients reported herein are estimated to be accurate within ± 0.010, and the estimated accuracy of the angle of attack is $\pm 0.1^{\circ}$.

Model Calibrations and Shake Tests

Static bending-moment calibrations.- The sensitivity of the bending bridge (millivolts output per inch-pound of applied bending moment) was determined by making static loadings of the wing and recording the bridge unbalance as indicated by the d-c millivolt meter. The linearity of the bridge output was determined by plotting the increase in bridge output as a function of the increase in applied load at any given loading point. The bridge output was found to be linear for all loading conditions, both positive and negative. The location of the effective bending axis was determined graphically from the results of the static load calibration. By moving a given load from point to point along individual loading lines, the actual effective bending axis was determined as the locus of loading points where the bridge output vanished. The location of the effective bending axis is shown in figure 8. The bridge was found to be essentially insensitive to torsion by comparing the results of identical loadings along various loading lines on the wing.

Shake tests.- The natural resonant frequencies of the model and sting-support system were determined by harmonically exciting the model at several points with an electromagnetic shaker. The output of the bending bridge and miniature movable accelerometers was monitored on an oscilloscope. A qualitative picture of the mode shapes involved was obtained by the use of the "1 g method" described in reference 5 and by traversing miniature accelerometers over the model and observing the amplitude and phase of their outputs. A sketch of the node lines associated with the various wing vibration modes is shown in figure 9.

An indication of the magnitude of the structural damping coefficients g for various vibration modes was obtained by suddenly removing the excitation and recording the decay of the bending bridge output for harmonic vibration in still air. Decay records were obtained for several initial stress amplitudes and an average value of g was determined.

Since the combined weight of the four mahogany wing bodies and three brass wing fences added to the wing panel was less than 5 percent of the weight of the basic wing panel, the changes in natural resonant frequencies and structural damping characteristics between the various configurations was negligible.

A listing of the model and support-system vibration modes, natural frequencies, and structural damping coefficients as obtained in still air is given in the following table:

Vibration mode	Resonant frequency, cps	Structural damping coefficient, g
Rigid body vertical translation	12	------
Rigid body rolling	17	0.0081
Rigid body pitching	23	.0080
First symmetrical wing bending	46	.0086
First antisymmetrical wing bending	79	.0047
Second symmetrical wing bending	124	.0107
Second antisymmetrical wing bending	205	.0192
Wing torsion	500	------

Wind-Tunnel Tests

The wind-tunnel tests were conducted over a Mach number range from 0.20 to 1.03. The angle-of-attack range was generally from -5° to 14° but was limited in some cases by model and balance maximum load limitations. In order to provide a reasonable angle-of-attack range and remain within maximum load limitations, the majority of the data were recorded at a free-stream total pressure of 0.4 atmosphere. Some data were obtained over a limited angle-of-attack range at a total pressure of 0.8 atmosphere. For the lower Mach numbers of 0.40 and 0.20 the free-stream total pressure was maintained at 1.0 and 2.0 atmospheres, respectively. A plot of the average Reynolds number (based on the wing mean aerodynamic chord of 7.08 inches) against Mach number at the various test total pressures is shown in figure 10.

REDUCTION OF DATA

During the wind-tunnel tests, the mean-square value of the random wing bending moment was continuously monitored on a thermocouple meter. Visual readings were taken at each data point. (The root-mean-square values thus derived were designated σ_{tc}.) The mean-square readings, which were a measure of the power involved in the entire frequency spectrum, provided an indication of the onset of buffeting and the overall buffet intensity but did not provide the information necessary for detailed investigation of the vibration modes involved. Therefore, the random time history of the buffet bending moment was simultaneously recorded on magnetic tape for those test conditions where the response was considered to be significant as indicated by the thermocouple meter. Power-spectral-density plots of the buffet response were derived from

the magnetic tape through the use of the analog equipment described in reference 6. Examination of the bending-moment spectra thus obtained revealed that approximately 95 percent of the power involved in the entire spectrum was limited to two wing modes and three rigid-body modes. (See fig. 11.) Fortunately, the three rigid-body modes involved were grouped and cleanly isolated in the frequency spectrum from the wing modes of importance. All of the power in the spectrum below a frequency of 30 cycles per second was associated with the rigid-body modes. The response in the rigid-body vertical translation and pitch modes was small for practically all test conditions. On the other hand, however, the response in the rigid-body rolling mode at approximately 17 cps was generally relatively large and at certain test conditions exceeded that at the first symmetrical wing-bending mode. This roll response was associated with the flexibility of the internally mounted six-component force balance in roll and the torsion characteristics of the sting-support system at the model.

In order to eliminate as much as possible of the spurious influence of the support-system flexibility contained in the data, a special high-pass filter was designed with a cutoff frequency of approximately 30 cps. After wind-tunnel tests had been completed, the magnetic-tape time-history records were played back through this filter, and thermocouple meter readings of the mean-square response were again taken. The root-mean-square values thus obtained were designated σ_f. In order to evaluate the effectiveness of the filter, a data point was chosen which indicated a large response in the rigid-body roll mode. This data point was analyzed both filtered and unfiltered and the result is shown in the form of power spectral density in figure 12. The response curve of the high-pass filter is also shown in figure 12. As indicated in figure 12, the filter did a very effective job of attenuating that portion of the power below a frequency of 30 cps. At the same time, however, some error was introduced into that portion of the spectrum immediately above 30 cps due to the fact that the filter could not have a perfectly sharp cutoff. The magnitude of this error is, of course, primarily a function of the power and damping involved in the first symmetrical wing-bending mode. The error in the root-mean-square bending moment for the spectrum shown in figure 12 was evaluated by integrating both the filtered and unfiltered spectrums over a frequency range from 30 to 140 cps and was found to be 4.8 percent. Root-mean-square values of the buffet bending moment derived from thermocouple-meter readings are presented both filtered and unfiltered in this paper. In addition to values derived from thermocouple meter readings, the root-mean-square buffet bending moment was also obtained by integrating the power-spectral-density plots. Values of total damping coefficient $\gamma + \frac{g}{2}$ were obtained from the power-spectral-density plots by the half-power method. That is, the total damping

coefficient was taken as one-half the bandwidth at the half-power point on the resonance peak divided by the resonant frequency of the peak.

Recordings of electronic instrumentation noise and the wing response to residual building vibration were made at various times throughout the investigation with no air flowing over the model. The equivalent root-mean-square bending moment was approximately 19 inch-pounds. This was considered to be a tare which could be subtracted from the data if desired.

RESULTS AND DISCUSSION

The lift characteristics of the various configurations which are presented in reference 3 are repeated here in figures 13(a) to 13(f) for convenience. An indication of the variation of buffet intensity with lift coefficient for each of the configurations is shown in figures 14(a) to 14(g) in terms of the root-mean-square values of the wing bending-moment fluctuations. The distinction between σ_{tc} and σ_f is discussed in the preceding section on reduction of data.

Wing buffeting is considered to be the response of an aerodynamically and structurally damped linear elastic system to externally applied random aerodynamic forces. The random wing response in the form of displacement or bending moment is thus a function of the structural characteristics of the system, the system damping, and the external exciting forces. Wing buffeting can be roughly classified as either stall buffet or shock-induced buffet. The former is excited, even at very low speeds, by the pressure fluctuations existing in the separated flow over the wing at high angles of attack near the stall. Shock-induced buffet, on the other hand, occurs at high subsonic and transonic speeds and can be excited at low lift conditions depending upon the strength and extent of the initial shock-wave formation on the wing. When the shock-wave—boundary-layer interaction is such that it causes the flow to separate, then the random flow field downstream of the shock excites buffeting vibrations which could present a serious structural problem.

In figure 14 the buffeting indicated at high lift coefficients for Mach numbers of 0.20, 0.40, and 0.60 is considered to be primarily stall buffeting and appears to be roughly proportional to the degree of penetration beyond the buffet-onset boundary. The erratic and large variation of buffet intensity at the higher subsonic and transonic Mach numbers for configurations 1 and 2 (figs. 14(a) and 14(b)) is considered to be primarily shock induced. For shock-induced buffeting, the magnitudes of the exciting forces generated on the surface of the wing depend

upon the increase in strength of the initial shock wave with increasing Mach number and upon any chordwise or spanwise movement of the shock pattern with increasing angle of attack and Mach number. Changes in the shock pattern on the wing produce changes in the amount and distribution of wing surface area which is bathed in shock-induced separated flow and thus directly affect the resultant wing buffet response. The detailed flow patterns on the surface of the wing at high lift conditions were not observed during this investigation and thus no explanation is available for the erratic behavior of the curves of figures 14(a) and 14(b) with increasing lift coefficient. However, the initial shock patterns which develop on relatively thick (8 to 12 percent chord) transport-type wings similar to the one used in this investigation (see, for example, ref. 7) can reasonably be expected to produce buffeting of the magnitude indicated in figures 14(a) and 14(b) with the exception of the unusually high peaks indicated at a Mach number of 0.93.

The exceptionally high peak at $M = 0.93$ for configurations 1 and 2 was the result of large harmonic vibrations of the model in the first antisymmetrical wing-bending mode. The wave form of the response, which occurred at almost a unique lift coefficient and angle of attack, was observed on a cathode-ray oscilloscope and recorded on magnetic tape during wind-tunnel tests. It appeared to be almost periodic at a frequency of 81.5 cps and the condition could be consistently repeated during testing. Possible causes of the unusually large response could have been (1) large antisymmetrical components in the external aerodynamic excitation, (2) the flexibility of the model and support system in roll, and (3) the relatively low aerodynamic and structural damping of the model in the particular mode of the response. This condition could not be made to occur for configurations 3 to 7 (figs. 14(c) to 14(g)) which incorporated special bodies added to the wing to reduce shock-induced separation.

Frequency Spectrum of Buffet Response

Shown in figures 15, 16, and 17 are typical power-spectral-density plots of the buffet response at various test conditions for configurations 1, 2, and 3, respectively. These plots were obtained by frequency analysis of the magnetic-tape data on the electronic analog equipment described in reference 8. The bandwidth of the scanning filter used was approximately 1.5 cps.

Approximately 85 percent of the power involved in the entire spectrum was confined to five vibration modes occurring in the frequency range from 0 to 100 cps. Of the three rigid-body modes (vertical translation, roll, and pitch) which occurred at frequencies below 30 cps, the roll mode was generally the only one which indicated significant

response. At several test conditions the response in this mode was comparable to or greater than that of the two primary wing modes. Of the two wing-vibration modes involved, the first symmetrical wing-bending mode which occurred at a frequency of approximately 46 cps was the only one which indicated significant response, with the exception of the unusually high peak response which occurred at $M = 0.93$ for configurations 1 and 2. In general, it will be observed that any significant increase or decrease in buffet intensity with lift coefficient for the various configurations as indicated by the curves of root-mean-square bending moment (fig. 14) is accompanied by a corresponding increase or decrease in the power involved in both the rigid body roll and first symmetrical wing bending modes.

Wing Damping Characteristics

Shown in figure 18 are the total damping coefficients $\gamma + \frac{g}{2}$ associated with the first symmetrical wing-bending mode for configurations 1 to 5. These total damping coefficients were inferred from the response power spectra by the use of the one-half power method. The accuracy of this method of evaluating the damping from the shape of the experimental buffet-response power spectrum depends upon the degree to which the system satisfies the following two assumptions: (1) the wing behaves like a single-degree-of-freedom system in the vicinity of the natural frequency of the first symmetrical bending mode and (2) the buffet input is independent of the frequency in the range where the output is significant. It can be seen from figures 15, 16, and 17 that the response peak associated with the first symmetrical wing-bending mode at approximately 46 cps was reasonably well isolated, in the frequency spectrum, from other modes of significant response. Therefore, the first assumption above appears to be reasonably satisfied. For the model used in this investigation, the frequency range of the first symmetrical-wing-bending-mode peak was so narrow that it is believed that the second assumption would be substantially satisfied by any reasonably smooth input spectrum.

An indication of the magnitude of the structural damping coefficient g for the various model natural vibration modes was derived from vibration decay records obtained from shake tests in still air. The value of g derived from the decay of harmonic vibrations in the first symmetrical wing-bending mode was approximately 0.0086. If this value for g was substituted into the values of total damping coefficient $\gamma + \frac{g}{2}$ plotted in figure 18 and the aerodynamic damping coefficient γ was solved for, then it would appear that the magnitude of the aerodynamic damping ranged from 2.5 to 8 times that of the structural damping.

Figure 18 indicates that the addition of wing bodies and fences to the model generally produced a desirable increase in the wing total damping at those lifting conditions where significant buffet response occurred. Since the variation in structural damping between the various configurations was very small for wind-off tests, it is believed that the increase in damping was primarily of the aerodynamic or viscous type.

Effects of Various Configuration Additions

Presented in figures 19 through 23 are comparison plots of the root-mean-square wing bending moment showing the changes in buffet intensity due to various configuration additions and modifications deemed desirable from an airplane performance and stability standpoint. The curves are faired through points which represent the total energy involved in the entire frequency spectrum. Also shown are flagged symbols which were derived by electronically filtering out the response in the rigid body modes and which represent only the energy involved in the wing modes. Also shown for comparison in figure 24 are buffet-onset boundaries for the various configurations. These boundaries were derived by considering the lift coefficient for buffet onset to be the point at which the curves of figure 14 first attained a slope of 45°. In order to provide a better indication of the areas in the Mach number—lift-coefficient plane where significant buffeting occurs, contours of constant buffet intensity as indicated by the root-mean-square wing-bending moment are plotted for the various configurations in figures 25(a) through 25(e). The buffet intensity contours for configurations 2, 3, and 4 are compared in figure 26. The buffet intensity levels indicated on the contour plots of figures 25 and 26 have been corrected for electronic recording instrumentation noise and wing response to residual building vibration recorded after wind-tunnel shutdown.

Effect of a fuselage addition.- By comparing configurations 1 and 2 in figures 19, 24, and 25(a) and (b), it can be seen that no consistent effect on the buffet intensity was produced by the fuselage addition. Figure 19 indicates that various response peaks were altered somewhat in magnitude but no consistent trend was discernible. The overall shape of the very erratic response curves in the speed range of shock-induced buffeting was very similar and indicates that both configurations experienced conditions of rather severe buffeting at the higher lift coefficients. Since the aerodynamic improvements to be realized by the fuselage addition are largely restricted to the inboard sections of the wing, no large change in the buffet characteristics was expected.

Effect of adding special bodies to the wing.- Comparison of the buffet response of configurations 2 (without wing bodies) and 3 (with wing bodies) in figures 20, 24, and 26 indicates that a marked reduction of buffet intensity and a delay of buffet onset at transonic speeds was achieved by the addition of specially contoured wing bodies. Figure 20 indicates that the rather large buffeting intensities for configuration 2 at Mach numbers from 0.90 to 1.03 were essentially eliminated by the incorporation of three inboard wing bodies on each wing panel. The unusually large peak response which occurred at $M = 0.93$ for configurations 1 and 2 (without wing bodies) could not be made to occur for any of the remaining configurations, all of which incorporated wing bodies. If the response in the rigid-body-roll mode is removed from the data (flagged symbols) for the configurations with wing bodies, then the remaining light buffeting is considered to be completely tolerable from the standpoint of strength considerations. It is believed that the marked improvement accomplished by the addition of the wing bodies was due to a large reduction in the magnitude of the external aerodynamic exciting forces caused by shock-induced separated flow and by an increase in the aerodynamic damping of the wing.

It is shown in figure 21 that the addition of a fourth wing body to the tip of each wing panel (in the presence of the three inboard wing bodies) produced no further improvements in the buffet characteristics.

Effect of adding wing fences.- Figures 22, 24, and 26 indicate that the fences produced substantial increases in buffet-onset lift coefficients at Mach numbers up to 0.90 and reduced the intensity of the stall buffeting which occurred at the high lift coefficients. At the higher transonic Mach numbers, however, a slight increase in the low-level buffet response was produced by the fences. (See fig. 22.) The improvement in buffet characteristics realized by fences as used in this investigation was, therefore, limited to the stall buffeting regime.

Effect of wing trailing-edge flaps.- Figure 23 shows the effects of adding 33- and 57-percent-semispan flaps to the wing trailing edges. The flaps were deflected 30° with respect to a plane perpendicular to the wing trailing edge. It can be seen that the addition of flaps increased the lift coefficients at which stall buffet occurred. Essentially no change in the low-lift response of the wing was produced by the deflected flaps.

SUMMARY OF RESULTS

The experimental wing buffet response of a transport-type airplane model with and without wing bodies, fences, flaps, and a fuselage

addition has been investigated at Mach numbers from 0.20 to 1.03. The wing had NACA 64A-series airfoil sections inclined 5° to the free-stream direction. The quarter-chord line of the wing was swept back 45°, the aspect ratio was 7, the taper ratio was 0.3, and the thickness ratio varied from 0.115 at the root to 0.075 at the midsemispan and was constant from that station to the tip. The wing was twisted and cambered for a design lift coefficient of 0.3.

The results of this investigation can be summarized as follows:

1. A marked reduction of buffet intensity and a delay of buffet onset at transonic speeds was achieved by the addition to the wing of special bodies designed to reduce shock-induced separation.

2. The further addition of wing fences produced substantial increases in buffet-onset lift coefficients at Mach numbers up to 0.90.

3. The addition of wing-trailing-edge flaps deflected 30° increased the lift coefficients at which low-speed stall buffeting occurred.

4. An addition to the fuselage near the upper forward portion produced no consistent change in the buffet characteristics.

Langley Research Center,
National Aeronautics and Space Administration,
Langley Field, Va., September 26, 1960.

REFERENCES

1. Whitcomb, Richard T.: Special Bodies Added on a Wing to Reduce Shock-Induced Boundary-Layer Separation at High Subsonic Speeds. NACA TN 4293, 1958.

2. Whitcomb, Richard T.: A Fuselage Addition To Increase Drag-Rise Mach Number of Subsonic Airplanes at Lifting Conditions. NACA TN 4290, 1958.

3. Loving, Donald L.: A Wind-Tunnel Investigation of a Transonic-Transport Configuration Utilizing Recent Drag-Improving Devices at Mach Numbers From 0.20 to 1.03. NASA TN D-636, 1961.

4. Kemp, William B., Jr., and King, Thomas J., Jr.: Wind-Tunnel Measurements of Wing Buffeting on 1/16-Scale Model of Douglas D-558-II Research Airplane. NACA RM L56G31, 1956.

5. Hanson, Perry W., and Tuovila, W. J.: Experimentally Determined Natural Vibration Modes of Some Cantilever-Wing Flutter Models by Using an Acceleration Method. NACA TN 4010, 1957.

6. Smith, Francis B.: Analog Equipment for Processing Randomly Fluctuating Data. Aero. Eng. Rev., vol. 14, no. 5, May 1955, pp. 113-119.

7. Whitcomb, Richard T.: An Experimental Study at Moderate and High Subsonic Speeds of the Flow Over Wings With 30° and 45° of Sweepback in Conjunction With a Fuselage. NACA RM L50K27, 1951.

TABLE I.- COORDINATES OF BASIC FUSELAGE AND FUSELAGE ADDITION

[All dimensions are in inches. (See fig. 3.)]

x	Basic fuselage	Fuselage addition		x	Basic fuselage	Fuselage addition	
	r	a	r_a		r	a	r_a
0	0			21.000	2.030	0.510	1.690
.100	.230			22.000	2.030	.415	1.710
.200	.350			22.500	2.030	.360	1.740
.400	.550			23.000	2.030	0	1.770
.600	.690			23.500	2.030		
.800	.800			24.000	2.030		
1.000	.910			24.500	2.030		
1.500	1.100			25.000	2.030		
2.000	1.260			26.000	2.030		
2.500	1.380			27.000	2.030		
3.000	1.480	0	1.300	28.000	2.030		
4.000	1.630	.220	1.460	29.000	2.030		
5.000	1.750	.250	1.570	30.000	2.028		
6.000	1.840	.320	1.660	31.000	2.024		
7.000	1.910	.400	1.720	32.000	2.019		
8.000	1.950	.480	1.765	33.000	2.012		
9.000	1.990	.560	1.810	34.000	2.000		
10.000	2.010	.655	1.830	35.000	1.980		
11.000	2.020	.740	1.855	36.000	1.963		
12.000	2.030	.830	1.860	37.000	1.933		
12.500	2.030	.870	1.860	38.000	1.896		
13.000	2.030	.920	1.860	39.000	1.849		
13.500	2.030	.960	1.860	40.000	1.788		
14.000	2.030	1.005	1.860	41.000	1.710		
14.500	2.030	1.050	1.855	42.000	1.618		
15.000	2.030	1.045	1.850	43.000	1.502		
15.500	2.030	1.000	1.845	44.000	1.375		
16.000	2.030	.945	1.835	45.000	1.261		
16.500	2.030	.900	1.825	46.000	1.176		
17.000	2.030	.850	1.810	47.000	1.130		
18.000	2.030	.750	1.765	47.140	1.128		
19.000	2.030	.650	1.740				
20.000	2.030	.595	1.690				

TABLE II.- COORDINATES OF BODIES ADDED TO THE WING

[All dimensions are in inches. (See fig. 5.)]

x	0.33 $\frac{b}{2}$	0.57 $\frac{b}{2}$	0.80 $\frac{b}{2}$	0.986 $\frac{b}{2}$
	r	r	r	r
0				0
.100			0	.034
.203		0	.060	.065
.268		.124	.068	.085
.500	0	.172	.102	.150
.781	.188	.239	.149	.220
1.000	.212	.282	.178	.267
1.250	.244	.336	.215	.310
1.500	.274	.387	.252	.345
2.000	.337	.482	.327	.386
2.500	.400	.570	.400	.400
3.000	.462	.644	.469	.380
3.500	.525	.704	.524	.332
3.750	.555	.725	.540	.298
4.000	.587	.741	.549	.255
4.500	.650	.767	.549	.158
5.000	.704	.783	.533	.038
5.150	.718	.787	.515	0
5.500	.748	.790	.500	
5.750	.763	.790	.475	
6.000	.778	.789	.446	
6.500	.791	.780	.375	
7.000	.799	.765	.282	
7.500	.800	.740	.166	
8.000	.795	.705	.022	
8.061	.794	.700	0	
8.500	.782	.660		
9.000	.761	.601		
9.350	.740	.550		
9.500	.729			
10.000	.686			
10.500	.630			
11.000	.565			
11.100	.550			

TABLE III.- WEIGHTS OF MODEL COMPONENTS

Component	Weight, lb
Basic fuselage and tail surfaces	36.14
Fuselage addition (mahogany and plastic)	.64
Strain-gage balance	4.25
One basic wing panel (steel):	
Inside fuselage	2.03
Outside fuselage	13.81
One wing body (mahogany) located at:	
0.33 semispan	.29
0.57 semispan	.25
0.80 semispan	.10
Wing tip	.03
One wing fence (brass) located at:	
0.33 semispan	.011
0.57 semispan	.009
0.80 semispan	.008
One wing flap (brass) extending from	
0.077-semispan station to:	
0.33-semispan station	.38
0.57-semispan station	.70

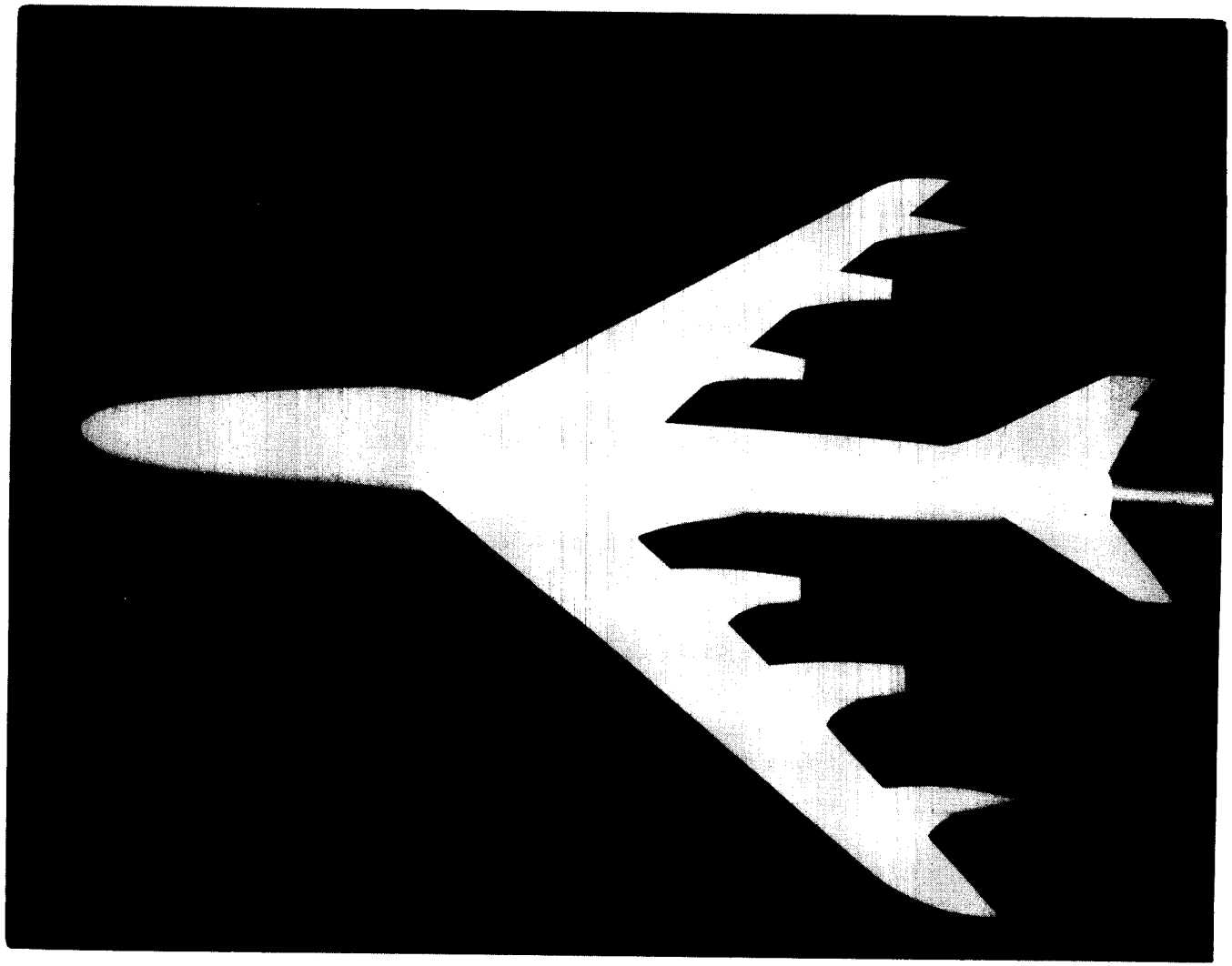

Figure 1.- Photograph of model (configuration 3). L-59-5125

Geometric characteristics of model

Wing:	
Airfoil section, root	Mod. NACA 64A011.5
Airfoil section, midsemispan to tip	Mod. NACA 64A007.5
Area, sq ft	2.0
Aspect ratio	7.0
Taper ratio	0.3
Sweepback of quarter-chord line, deg	45
Incidence, deg	2
Dihedral, deg	6
Horizontal tail:	
Airfoil section	NACA 65A006
Area, sq ft	0.33
Aspect ratio	3.0
Taper ratio	0.3
Sweepback of quarter-chord line, deg	45
Vertical tail:	
Airfoil section	NACA 65A006
Area (without dorsal fairing), sq ft	0.25
Aspect ratio	1.5
Taper ratio	0.26
Sweepback of quarter-chord line, deg	45

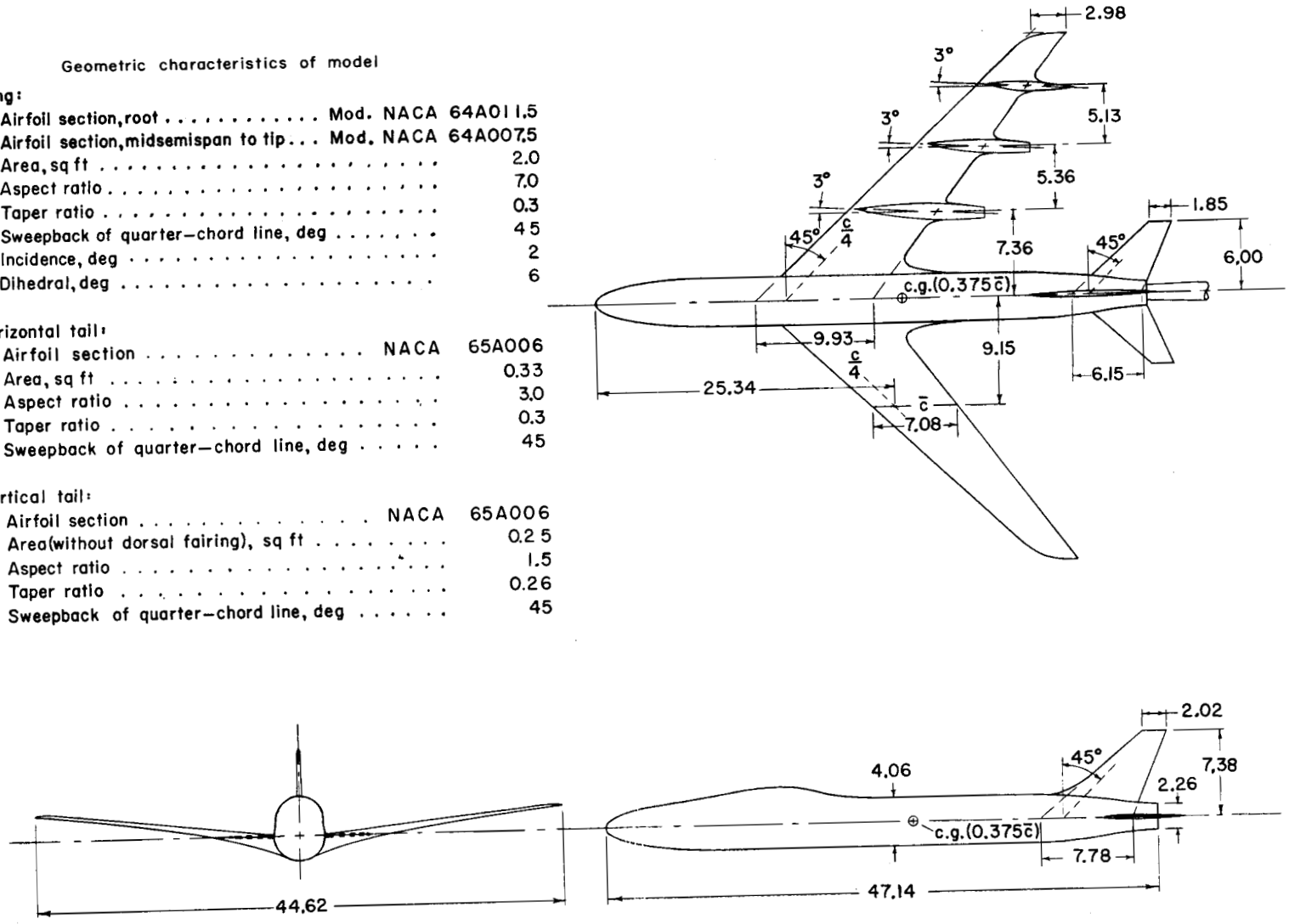

Figure 2.- Three-view drawing of the model. All linear dimensions are in inches.

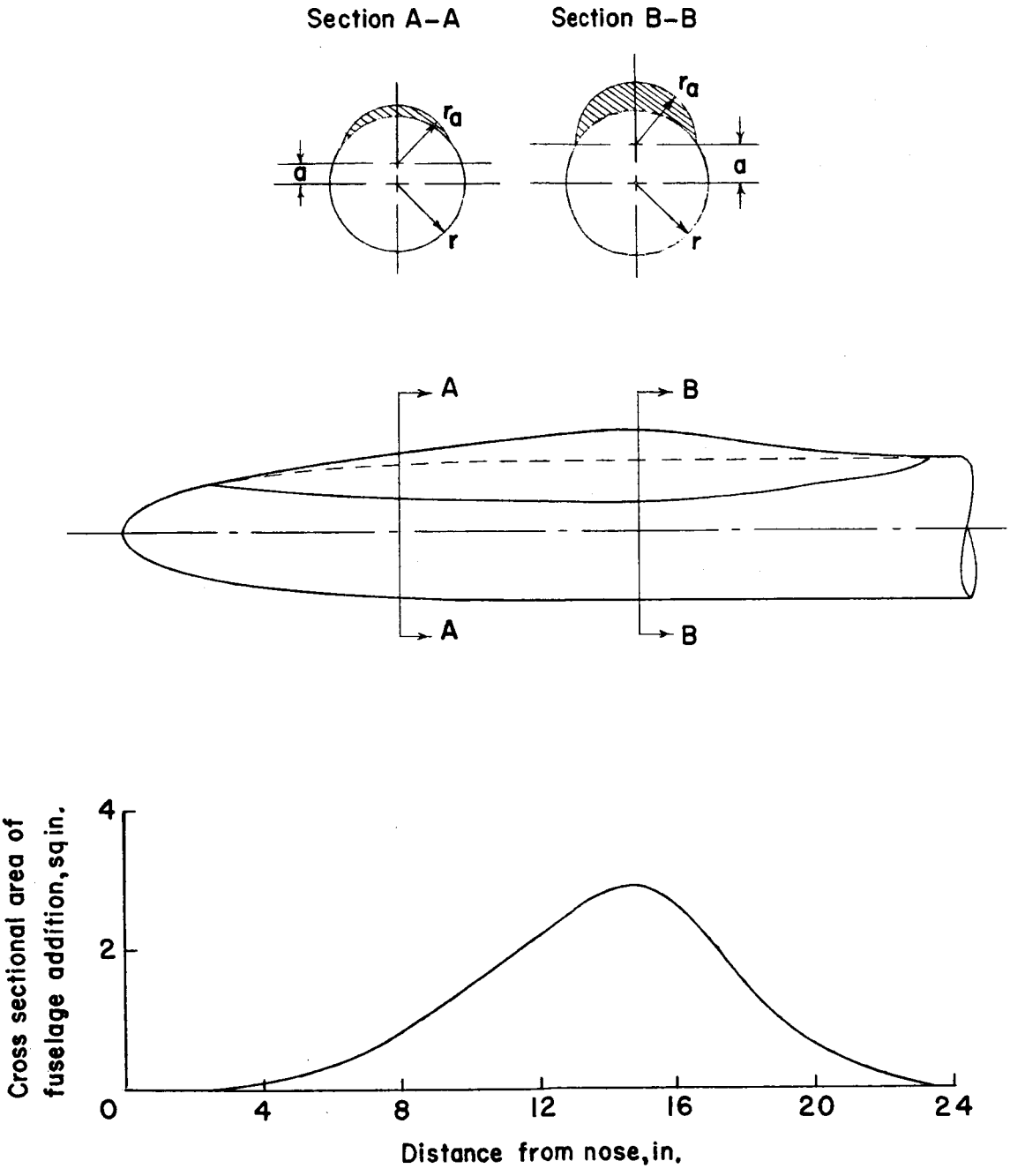

Figure 3.- Sketch of details of fuselage addition.

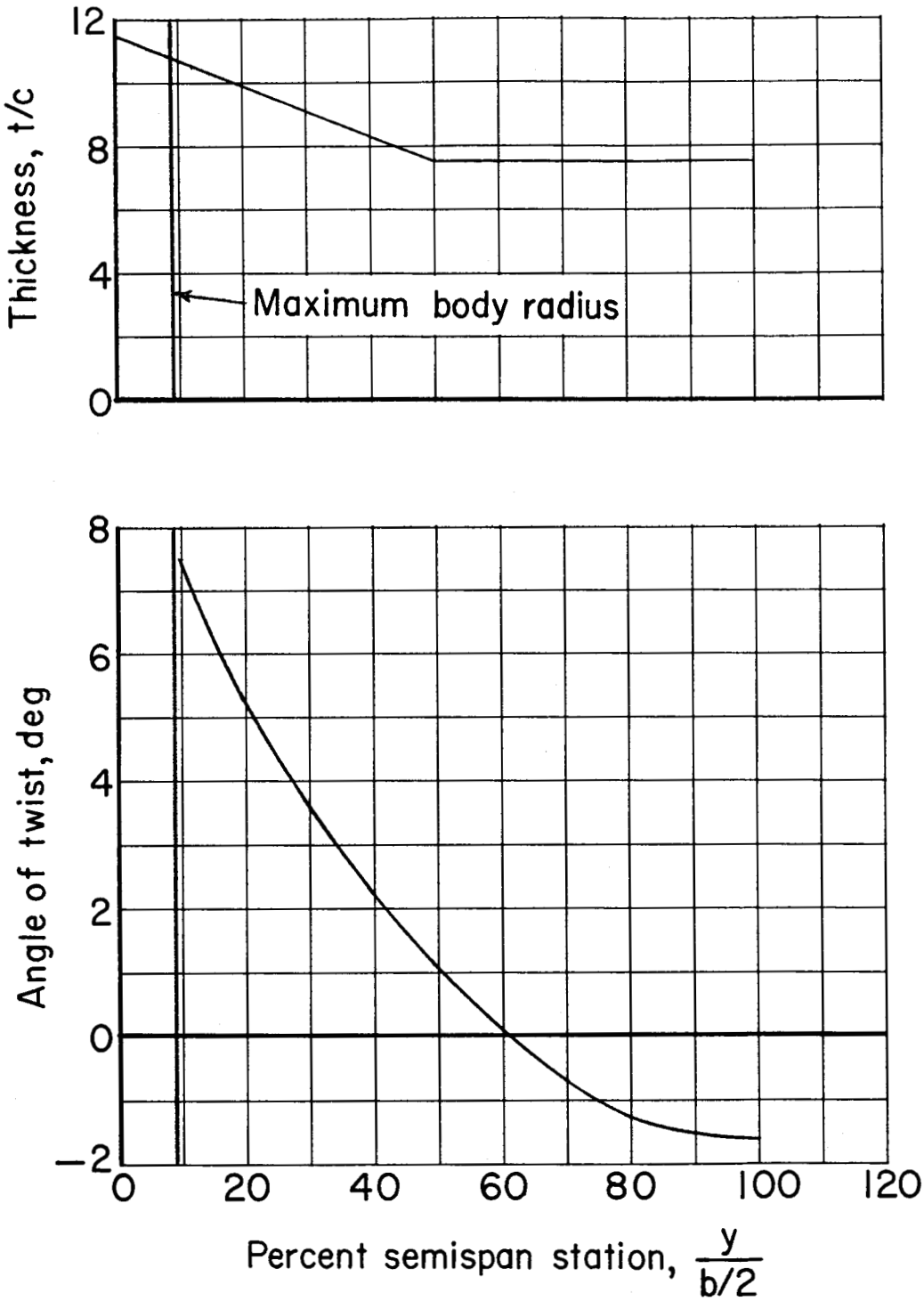

Figure 4.- Model wing twist and thickness distributions.

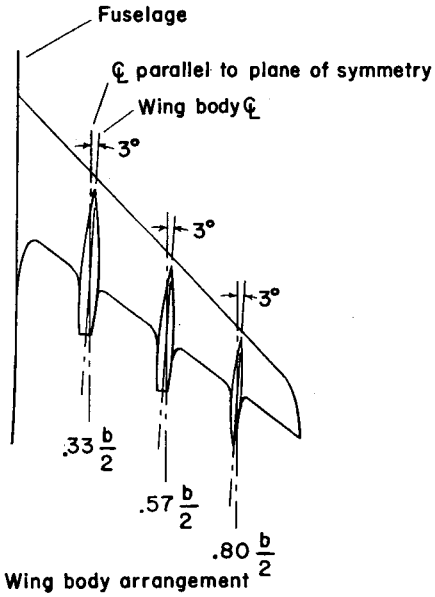

Wing body arrangement

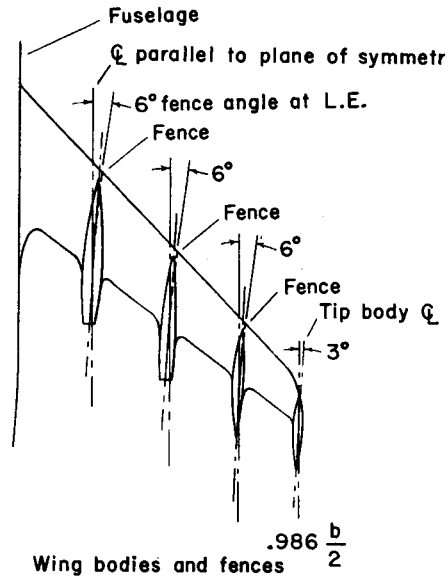

Wing bodies and fences

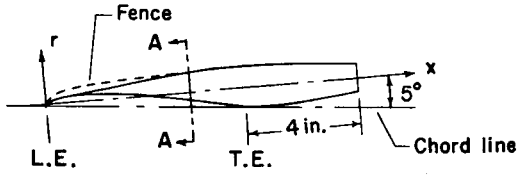

Station 0.33 b/2

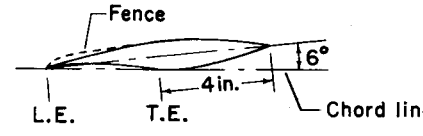

Station 0.80 b/2

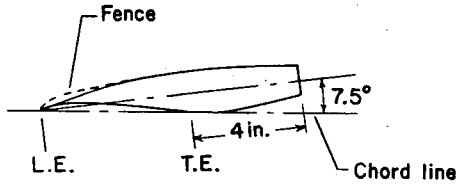

Station 0.57 b/2

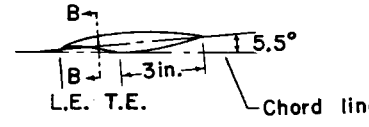

Station 0.986 b/2

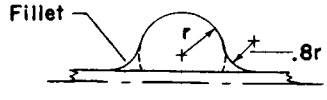

Section A–A (typical)
Not to scale

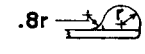

Section B–B
Not to scale

Figure 5.- Details of added wing bodies and fences.

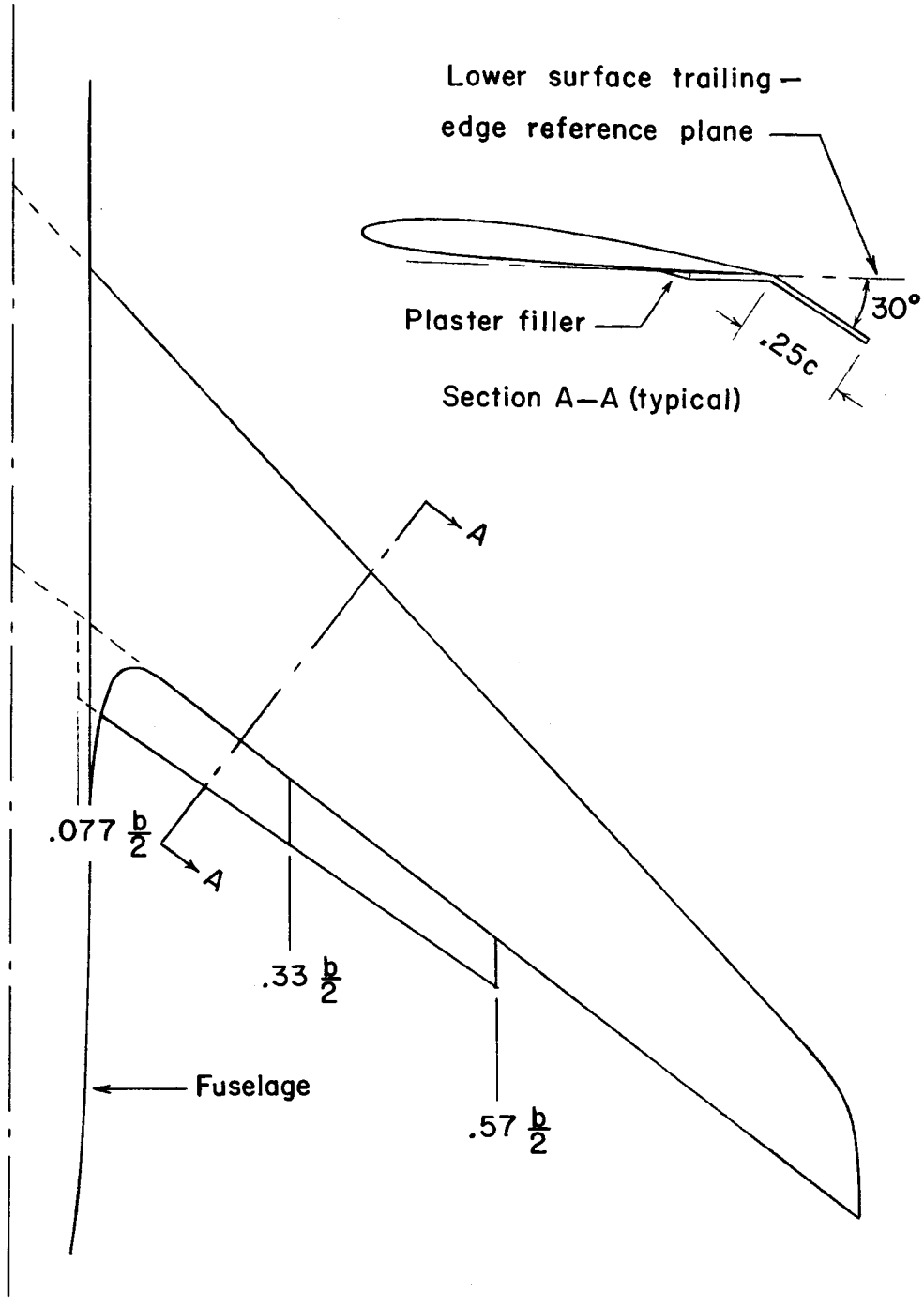

Figure 6.- Details of wing trailing-edge-flap installation.

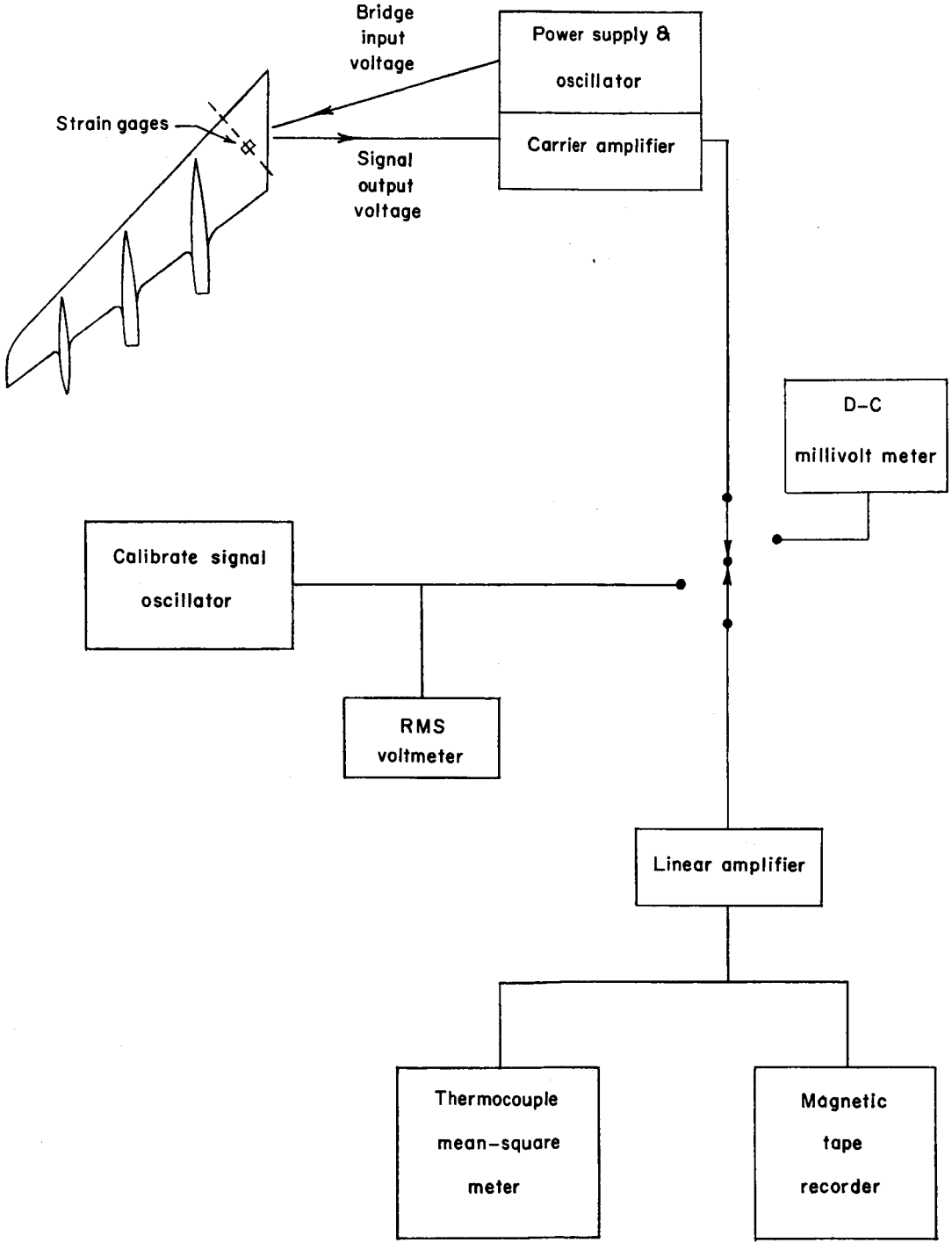

Figure 7.- Block diagram of instrumentation used to record buffet data.

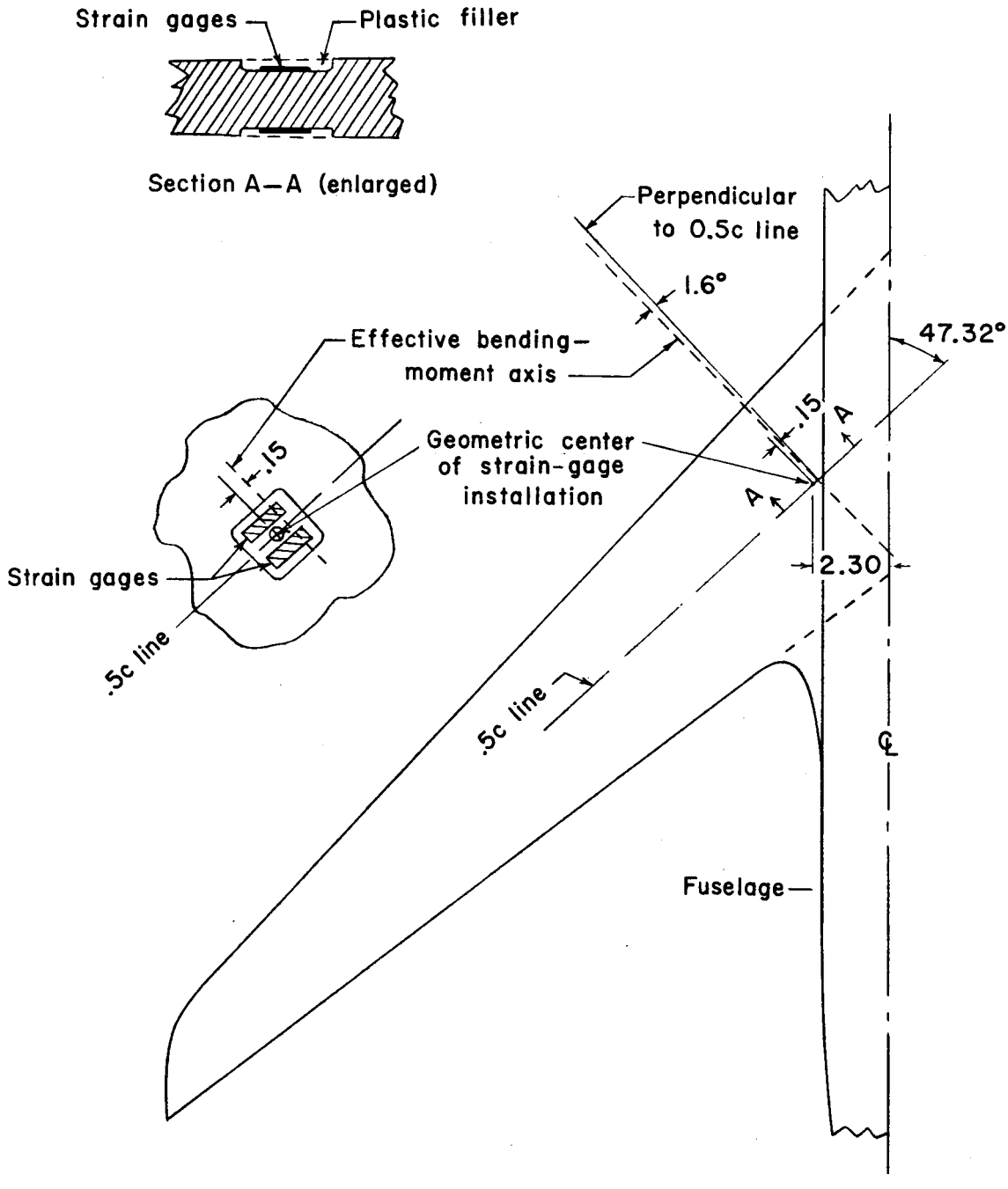

Figure 8.- Details of wing strain-gage installation and location of the effective bending axis. All linear dimensions are in inches.

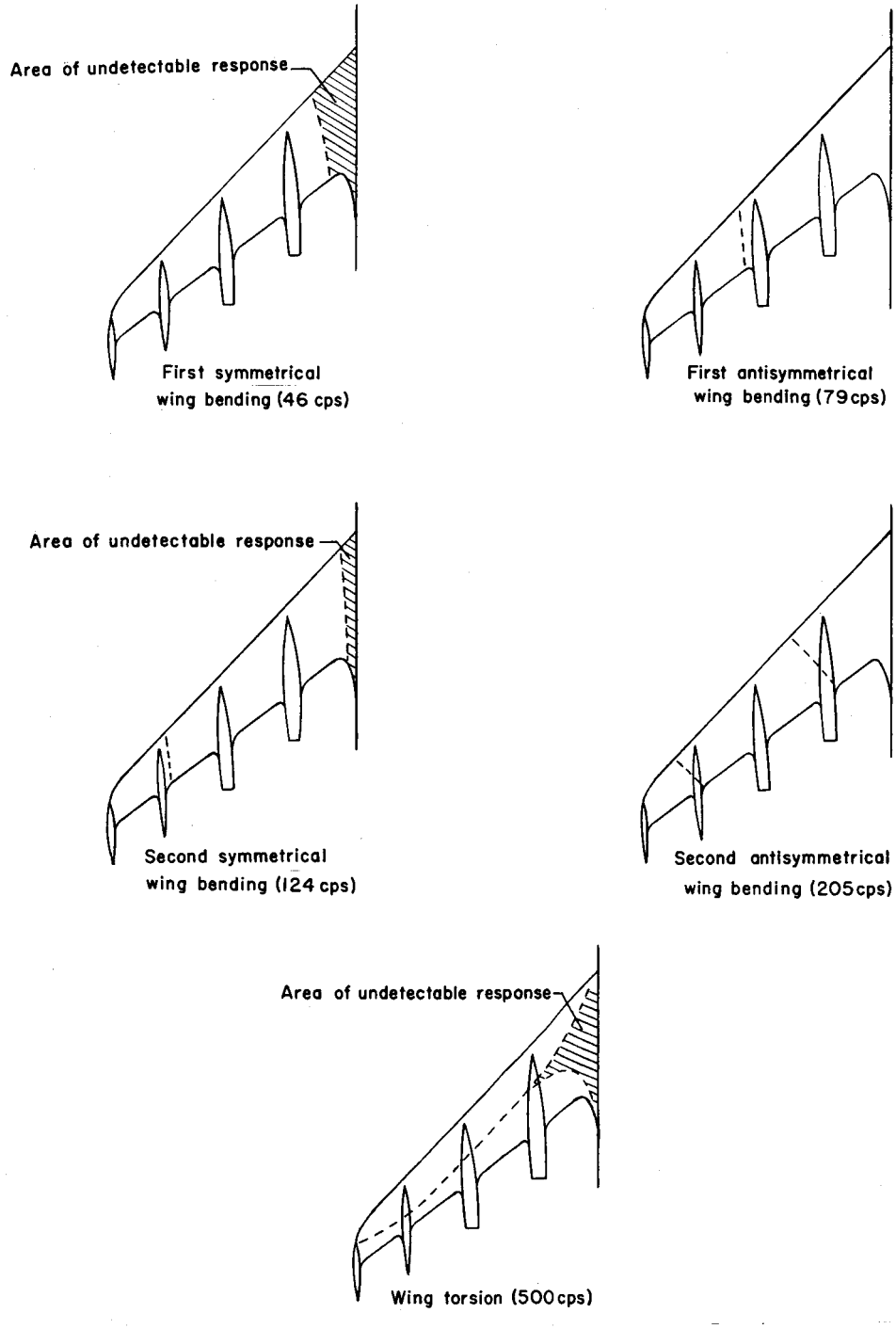

Figure 9.- Sketch of the node lines associated with the various wing vibration modes.

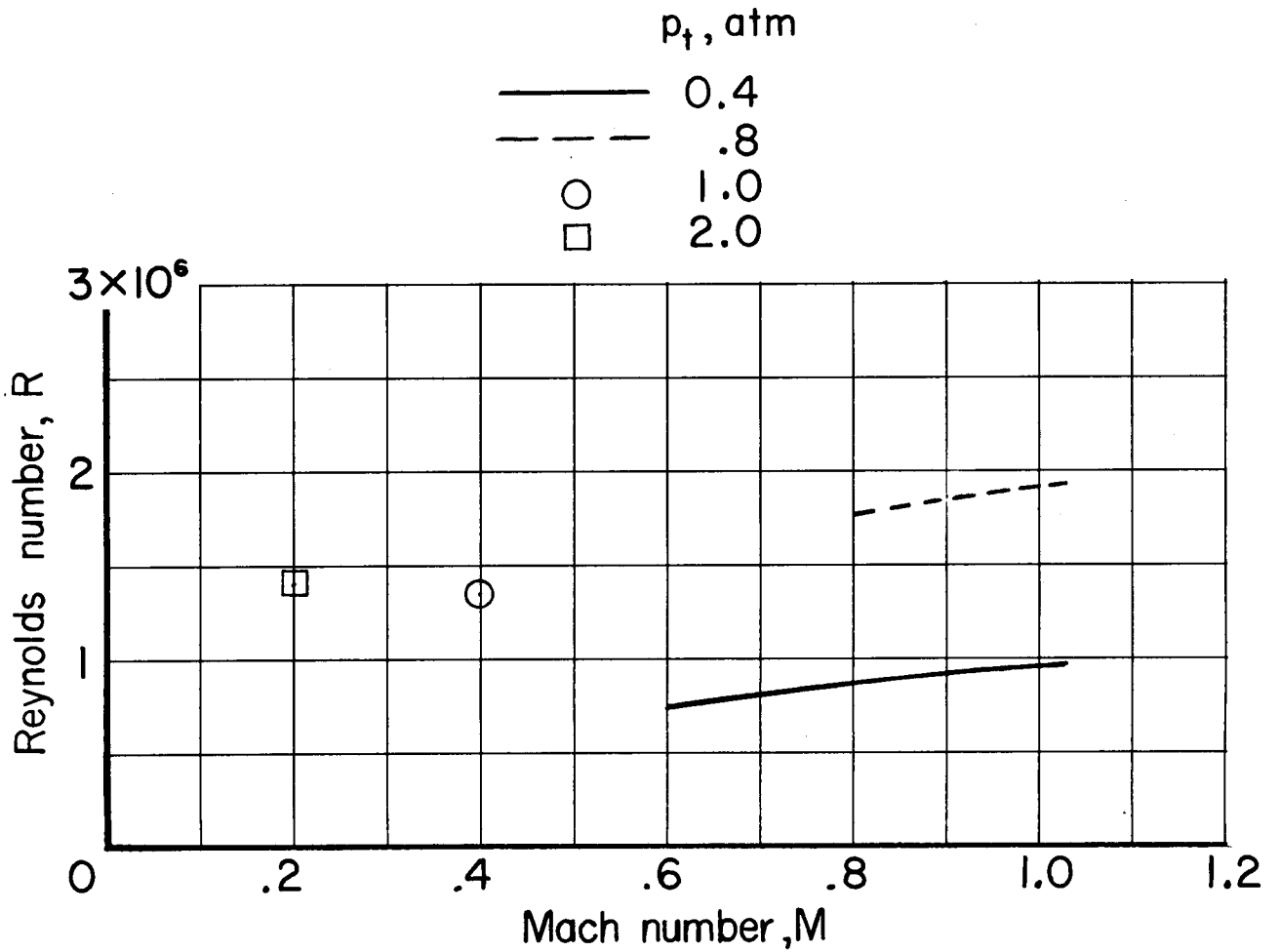

Figure 10.- Average Reynolds number (based on wing mean aerodynamic chord of 7.08 in.) for the various test total pressures.

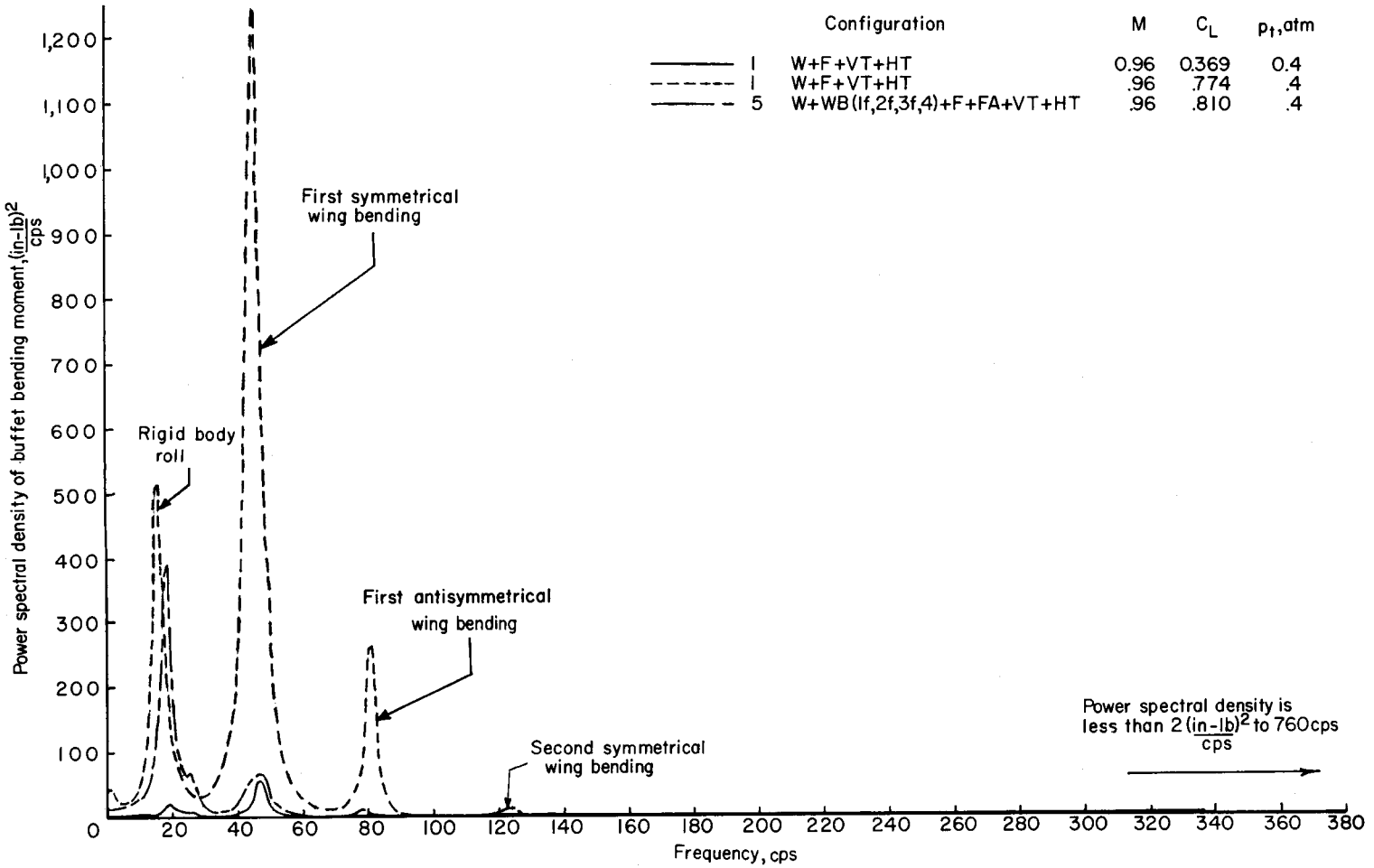

Figure 11.- Typical spectra of the output of the bending-moment gage with a filter bandwidth of approximately 4.5 cycles per second.

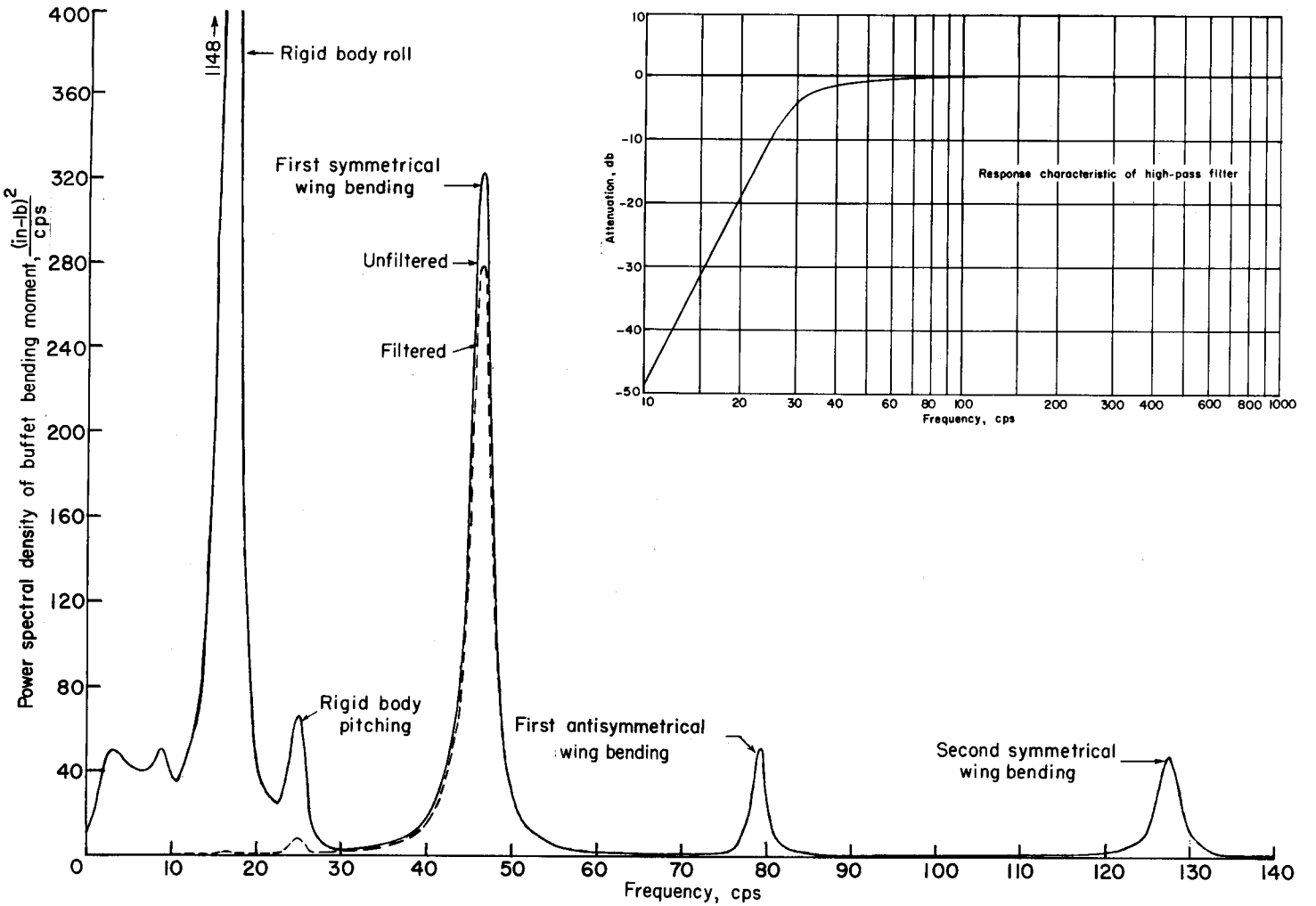

Figure 12.- Evaluation of the effectiveness of a high-pass filter designed to eliminate the buffet response due to model-support system. (The effective bandwidth of the scanning bandpass filter used in the analysis was approximately 1.8 cps.)

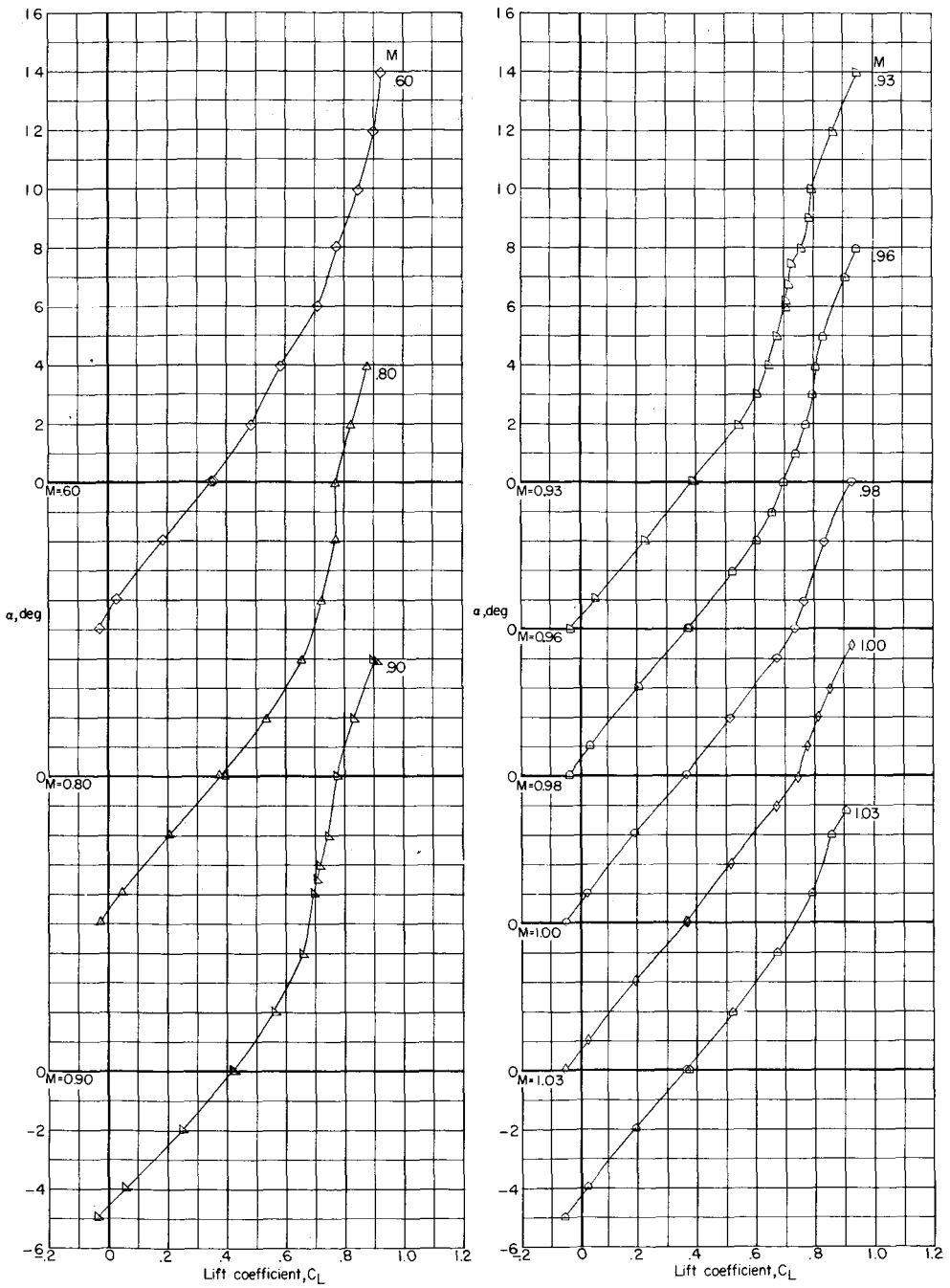

(a) Configuration 1 (W + F + VT + HT).

Figure 13.- Lift characteristics of the various configurations (from ref. 3). p_t = 0.4 atm except as indicated.

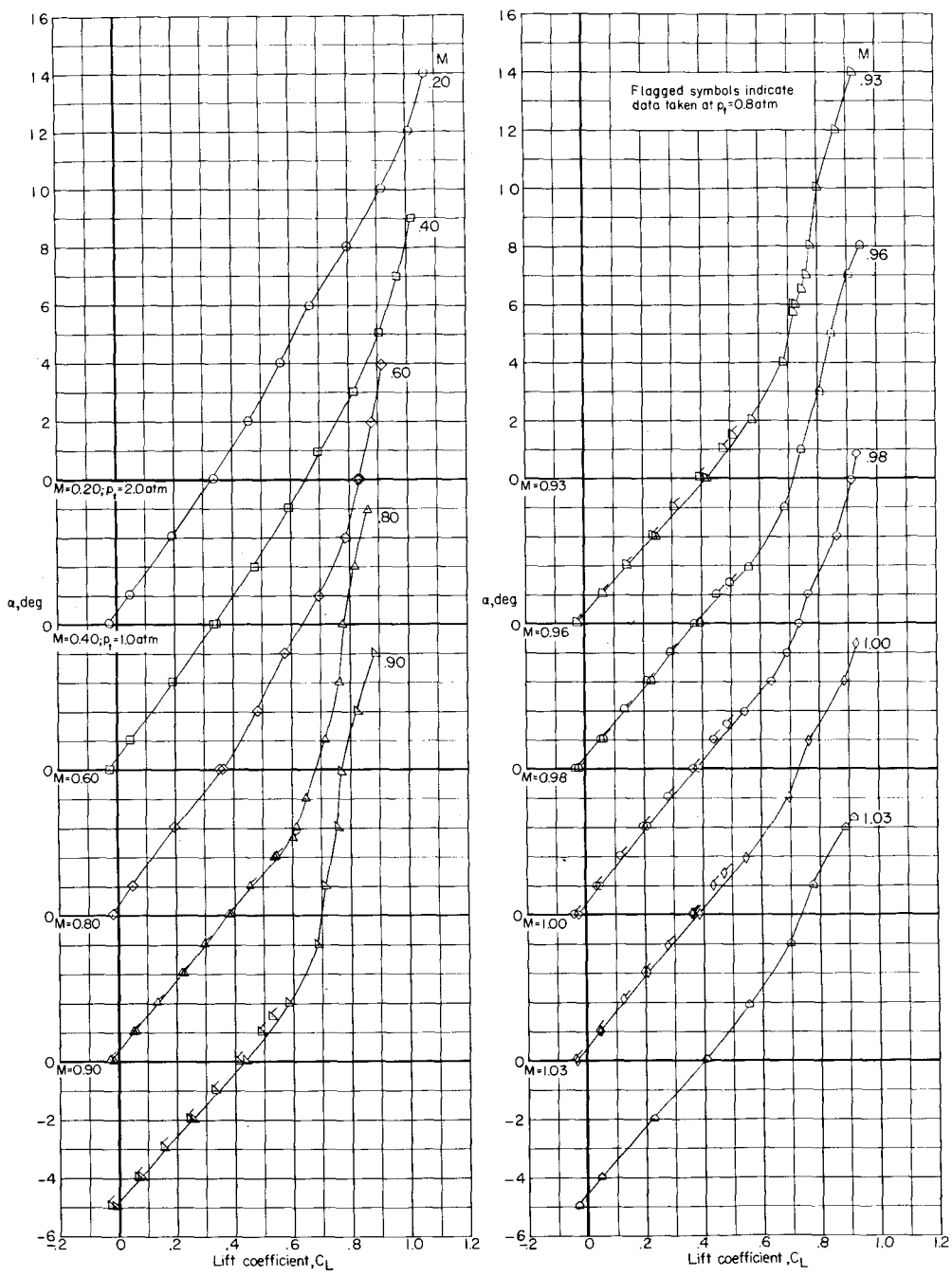

(b) Configuration 2 (W + F + FA + VT + HT).
Flagged symbols indicate data taken at p_t = 0.8 atm.

Figure 13.- Continued.

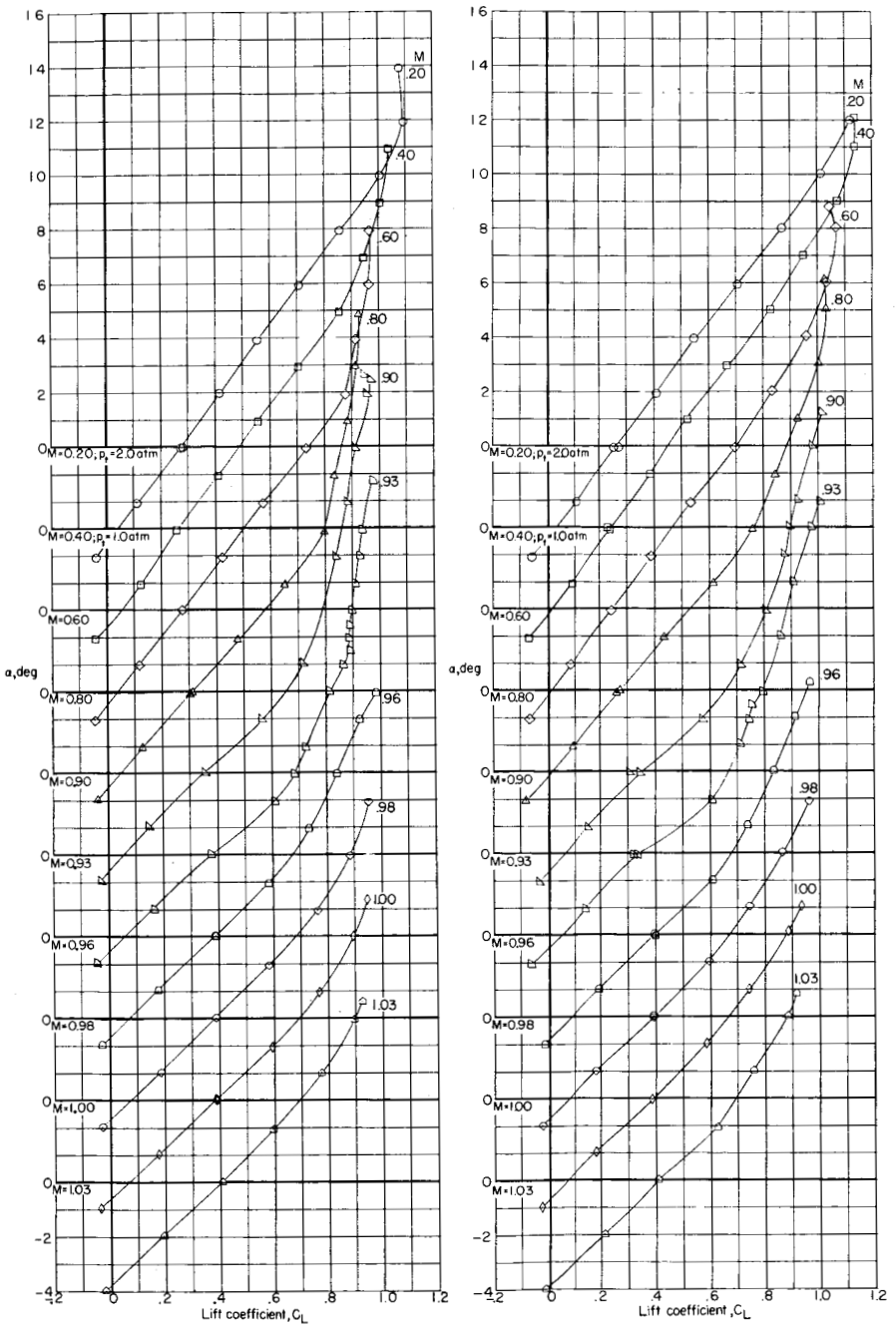

(c) Configuration 3
(W+ WB(1, 2, 3) + F+ FA+ VT +HT).

(d) Configuration 4
(W+ WB(1f, 2f, 3f,)+ F +FA+ VT+ HT).

Figure 13.- Continued.

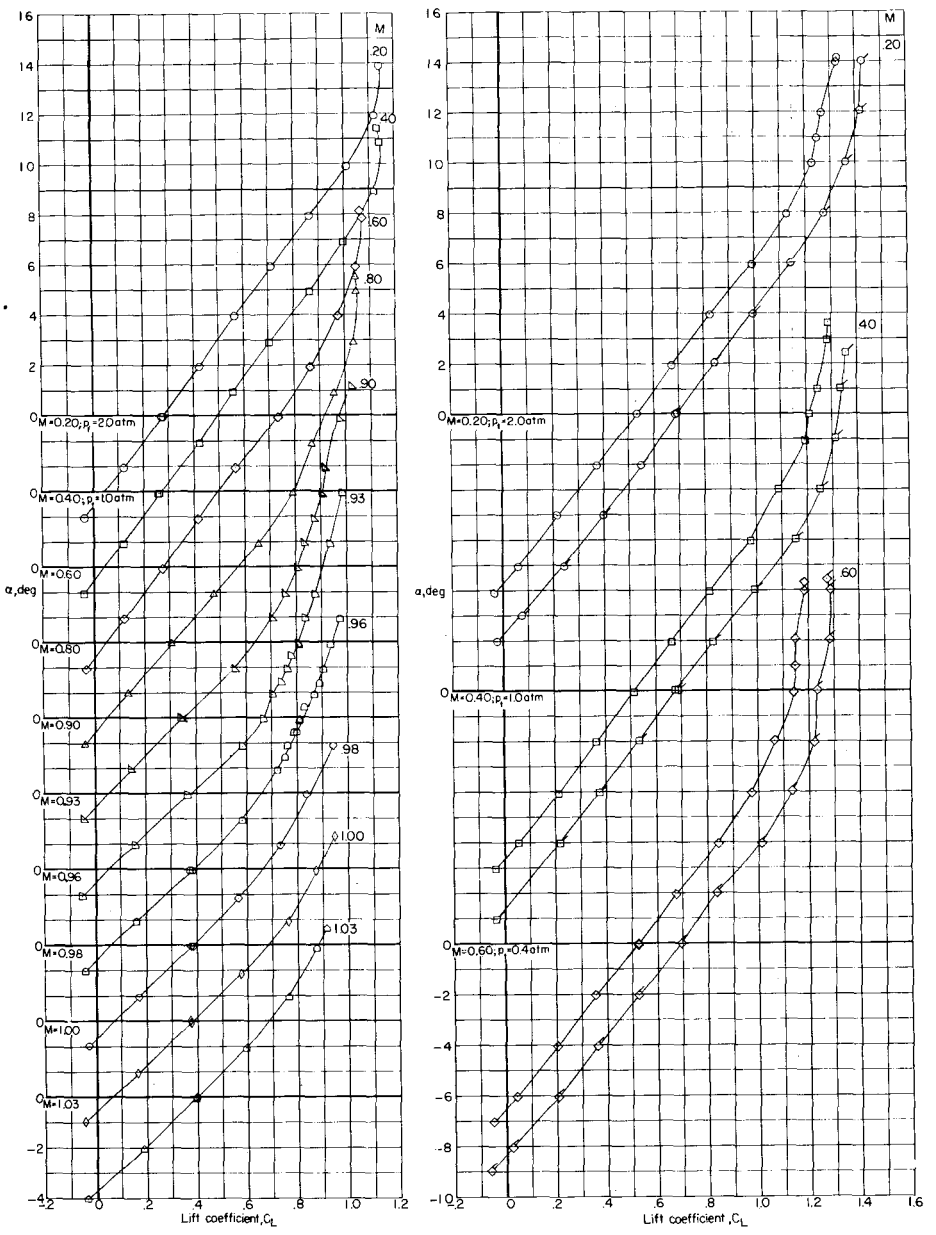

(e) Configuration 5 (W + WB(1f, 2f, 3f, 4) + F + FA + VT + HT).

(f) Configuration 6 (W + WB(1f, 2f, 3f) + WF(.33 semispan) + F + FA + VT + HT). (Plain symbols.) Configuration 7 (W + WB(1f, 2f, 3f) + WF(.57 semispan) + F + FA + VT + HT). (Flagged symbols.)

Figure 13.- Concluded.

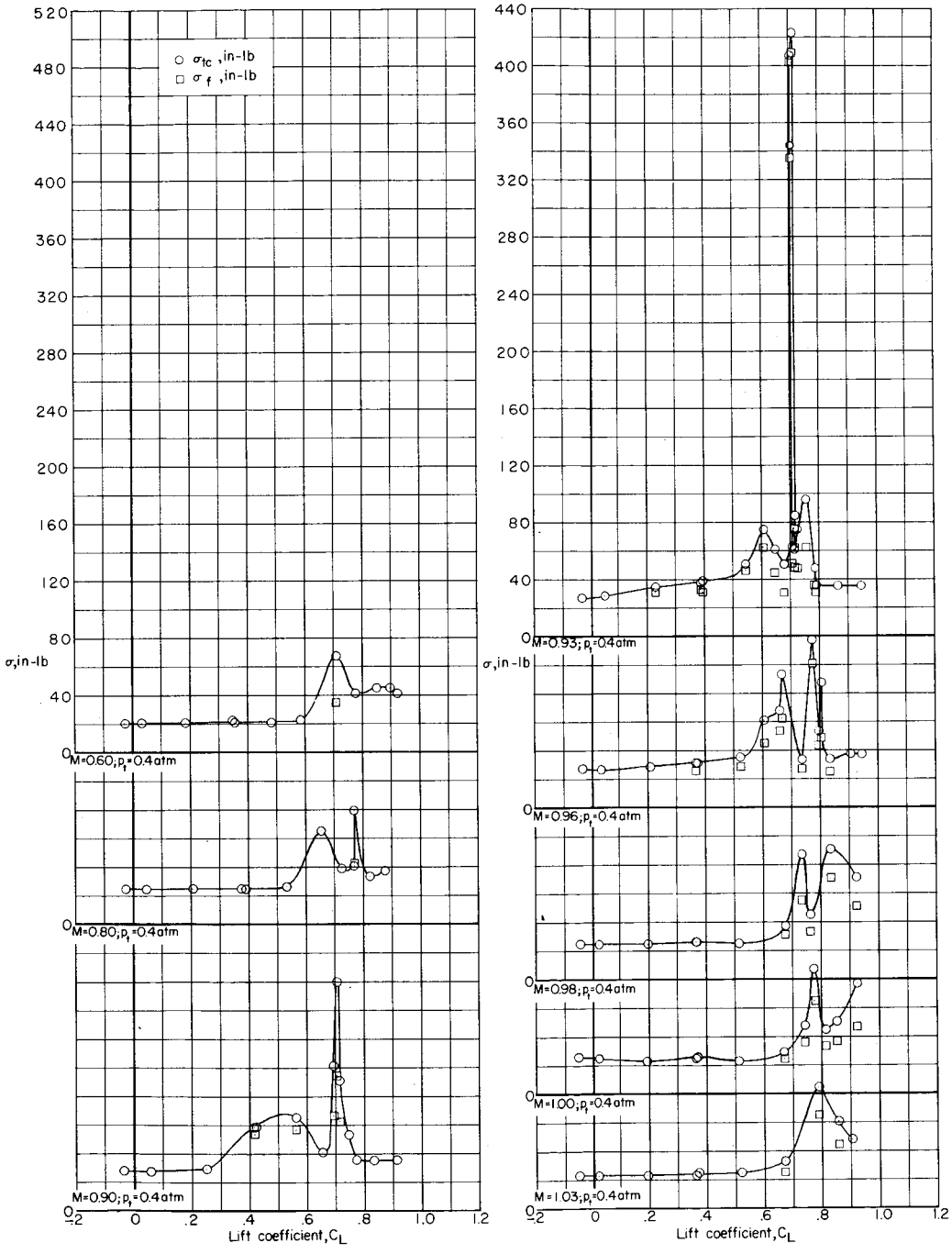

(a) Configuration 1 (W + F + VT + HT).

Figure 14.- Root-mean-square wing bending-moment fluctuations due to buffeting versus lift coefficient for the various configurations.

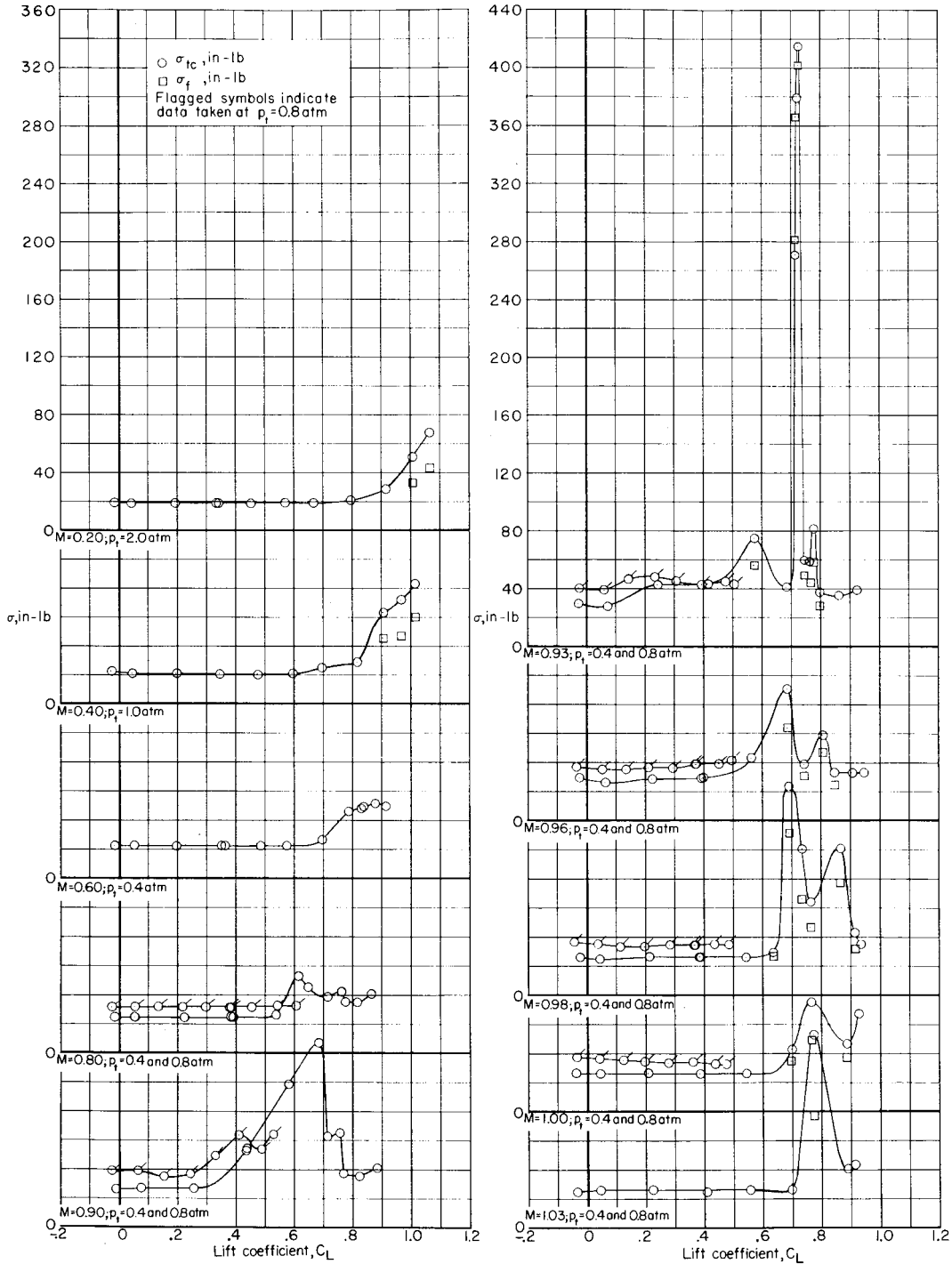

(b) Configuration 2 (W + F + FA + VT + HT).

Figure 14.- Continued.

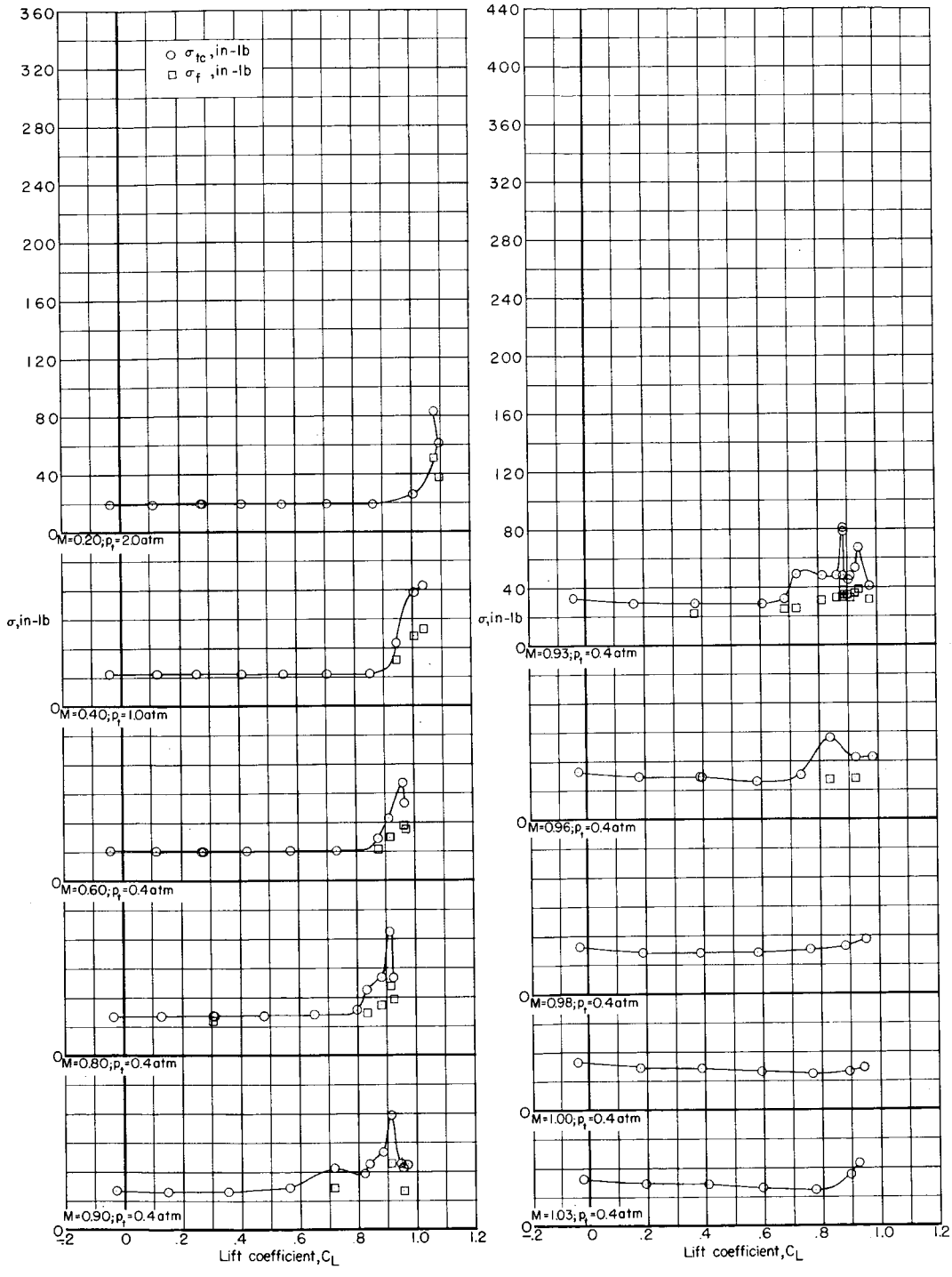

(c) Configuration 3 (W + WB(1, 2, 3) + F + FA + VT + HT).

Figure 14.- Continued.

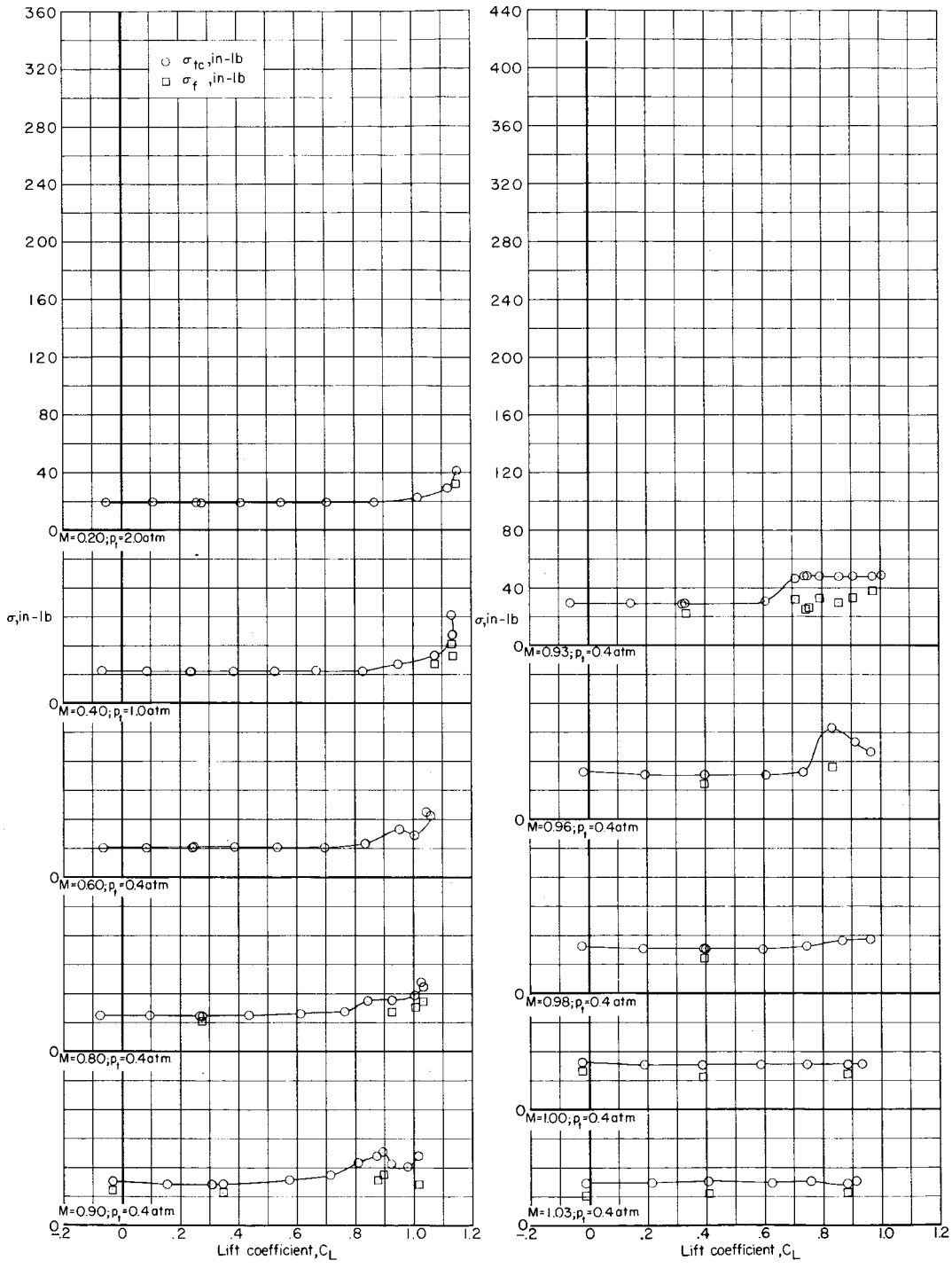

(d) Configuration 4 (W + WB(1f, 2f, 3f) + F + FA + VT + HT).

Figure 14.- Continued.

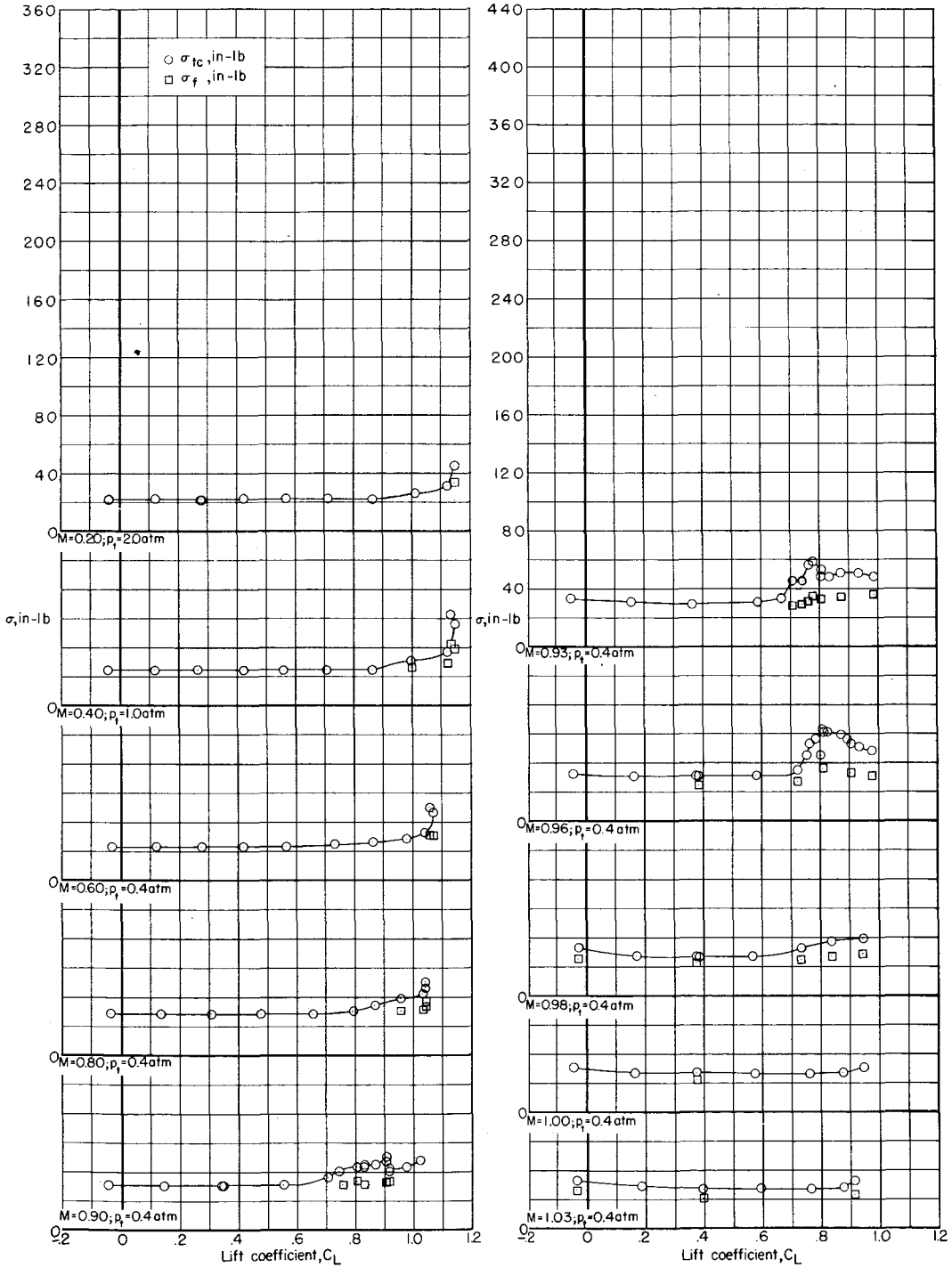

(e) Configuration 5 (W + WB(1f, 2f, 3f, 4) + F + FA + VT + HT).

Figure 14.- Continued.

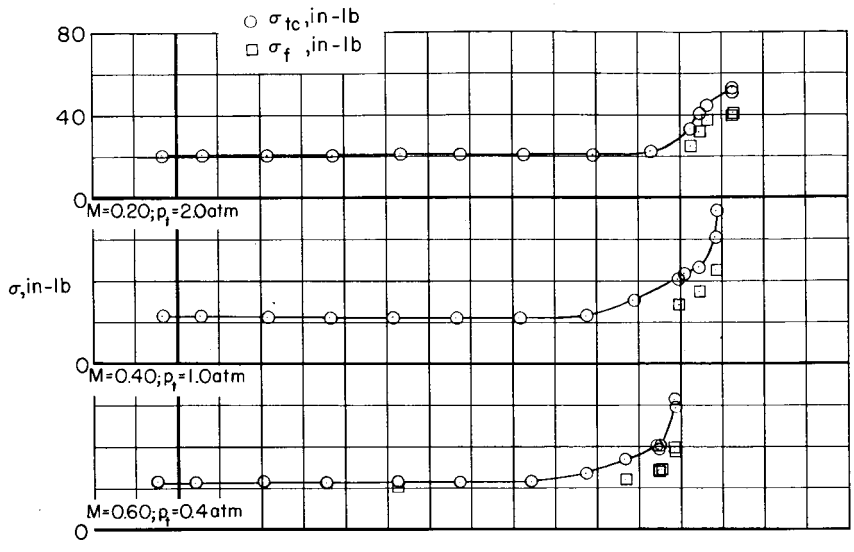

(f) Configuration 6 (W + WB(1f, 2f, 3f) + WF(.33 semispan) + F + FA + VT + HT).

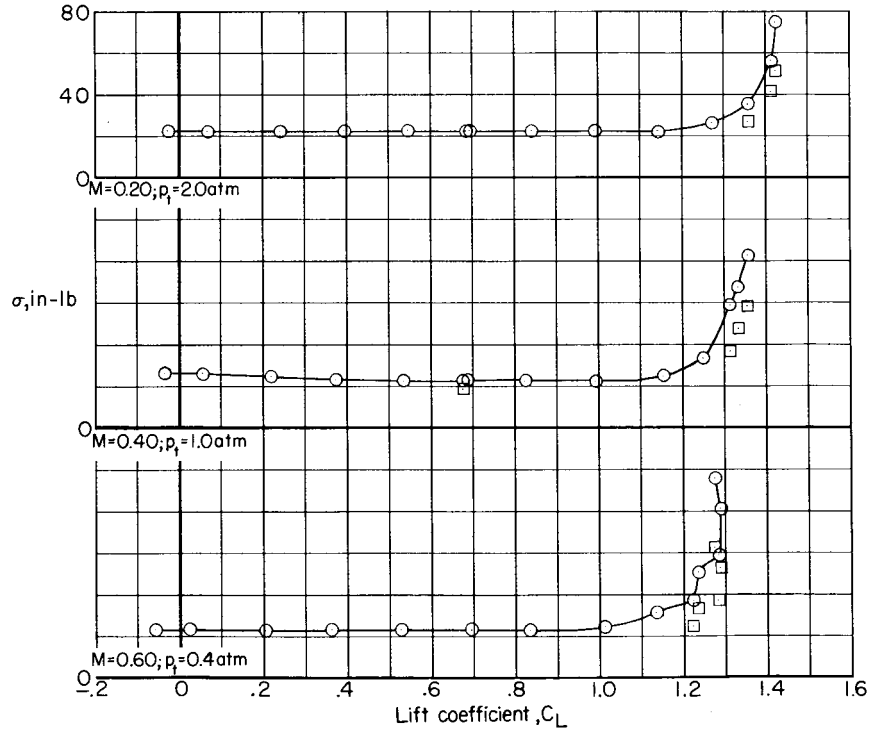

(g) Configuration 7 (W + WB(1f, 2f, 3f) + WF(.57 semispan) + F + FA + VT + HT).

Figure 14.- Concluded.

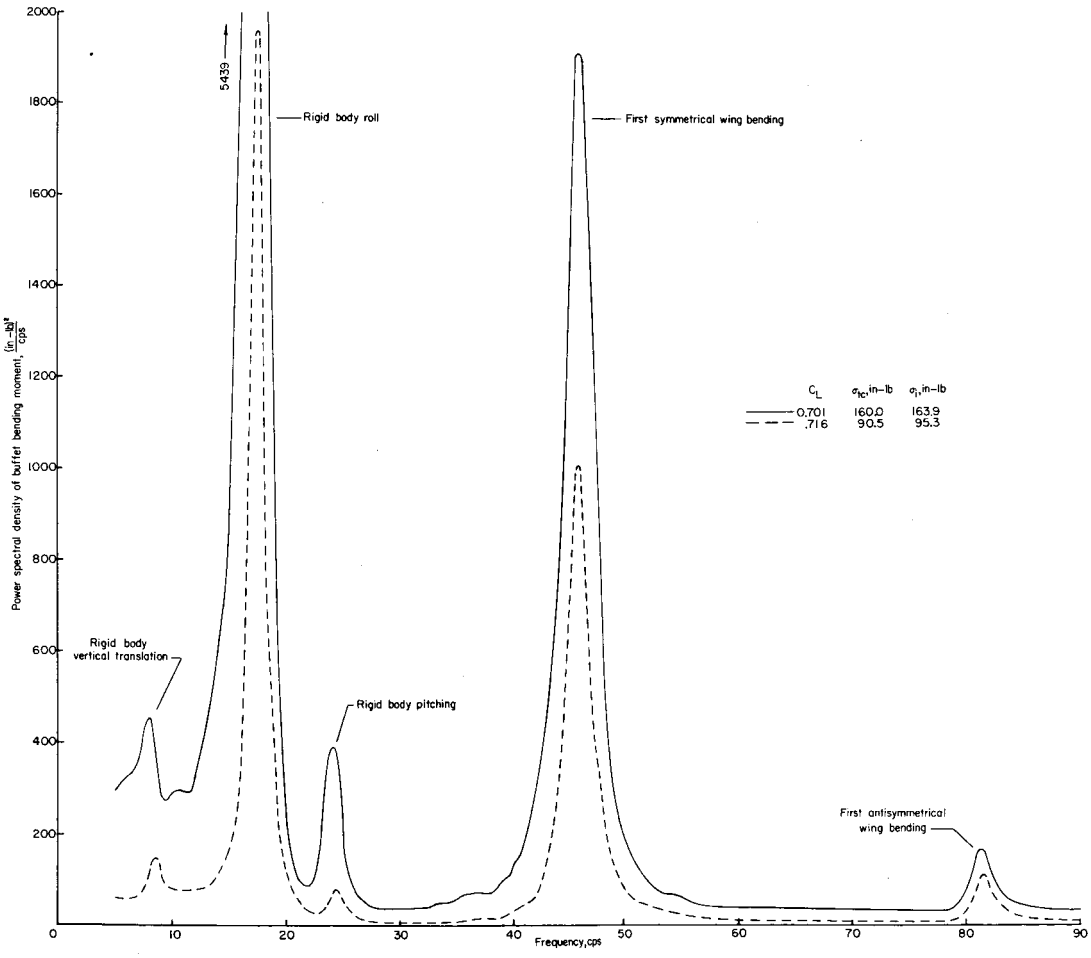

(a) M = 0.90; p_t = 0.4 atm.

Figure 15.- Power spectral density of buffet response at various test conditions for configuration 1 (W + F + VT + HT). (Effective bandwidth of scanning bandpass filter was approximately 1.5 cps.)

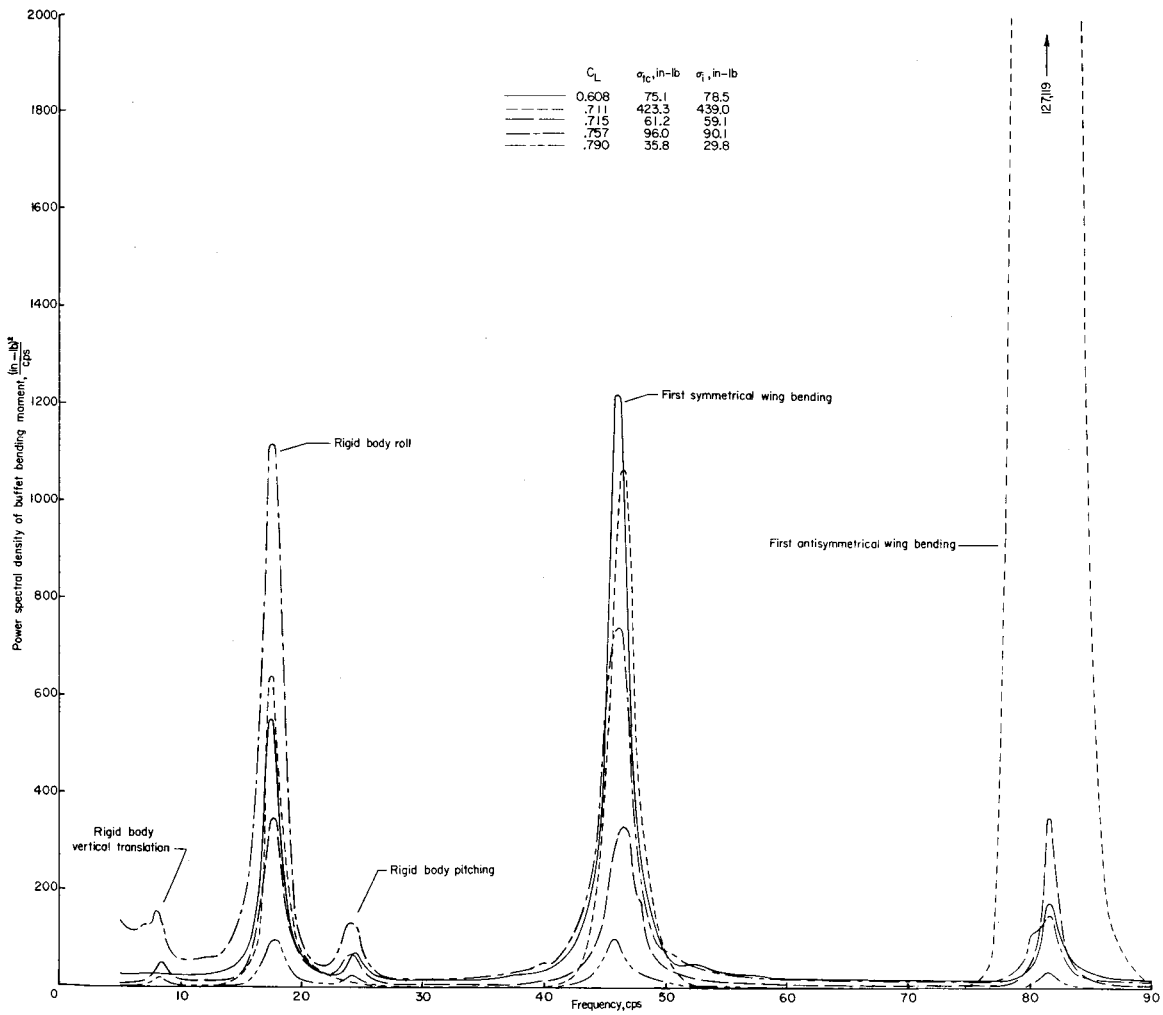

(b) M = 0.93; p_t = 0.4 atm.

Figure 15.- Continued.

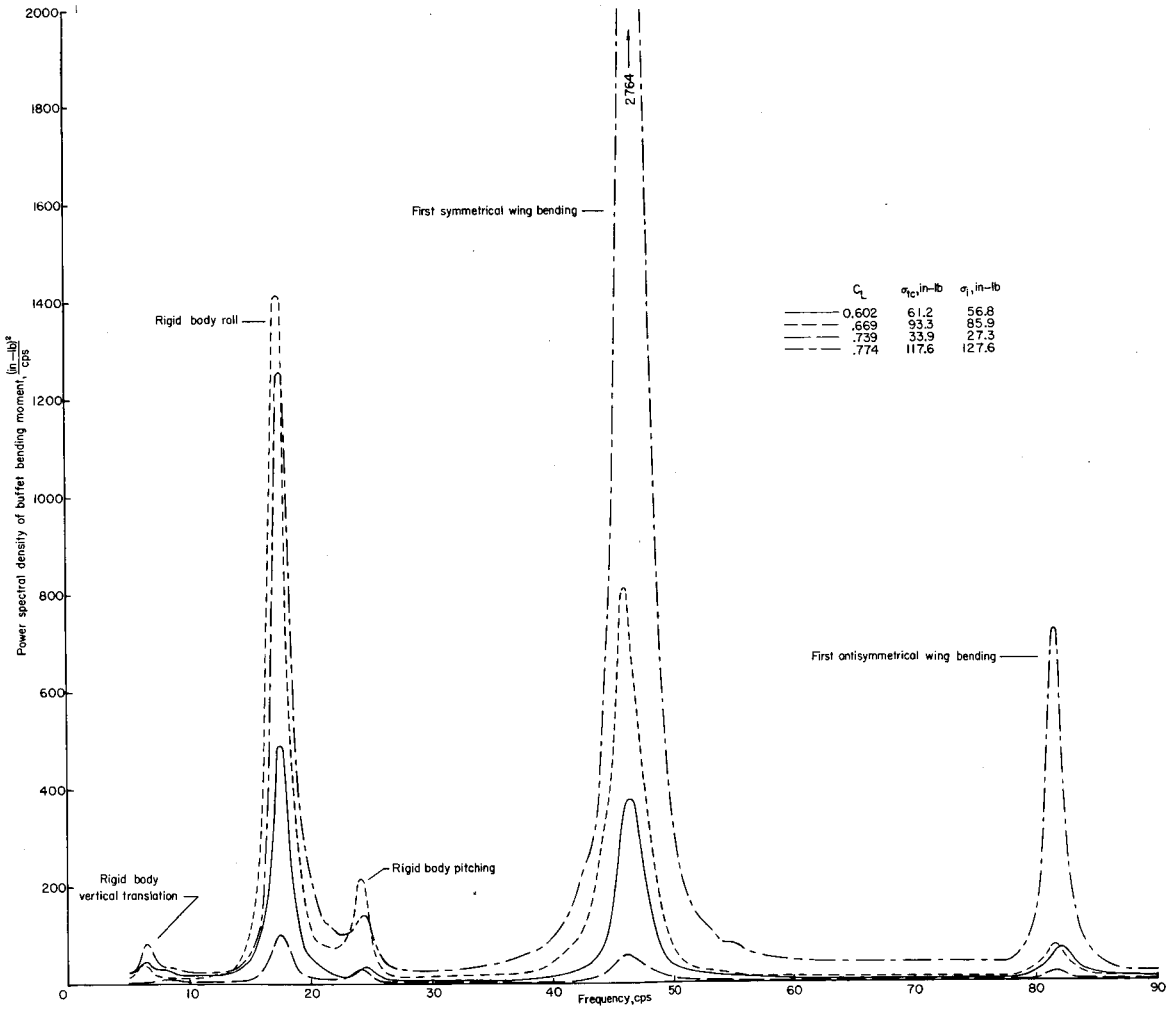

(c) M = 0.96; p_t = 0.4 atm.

Figure 15.- Continued.

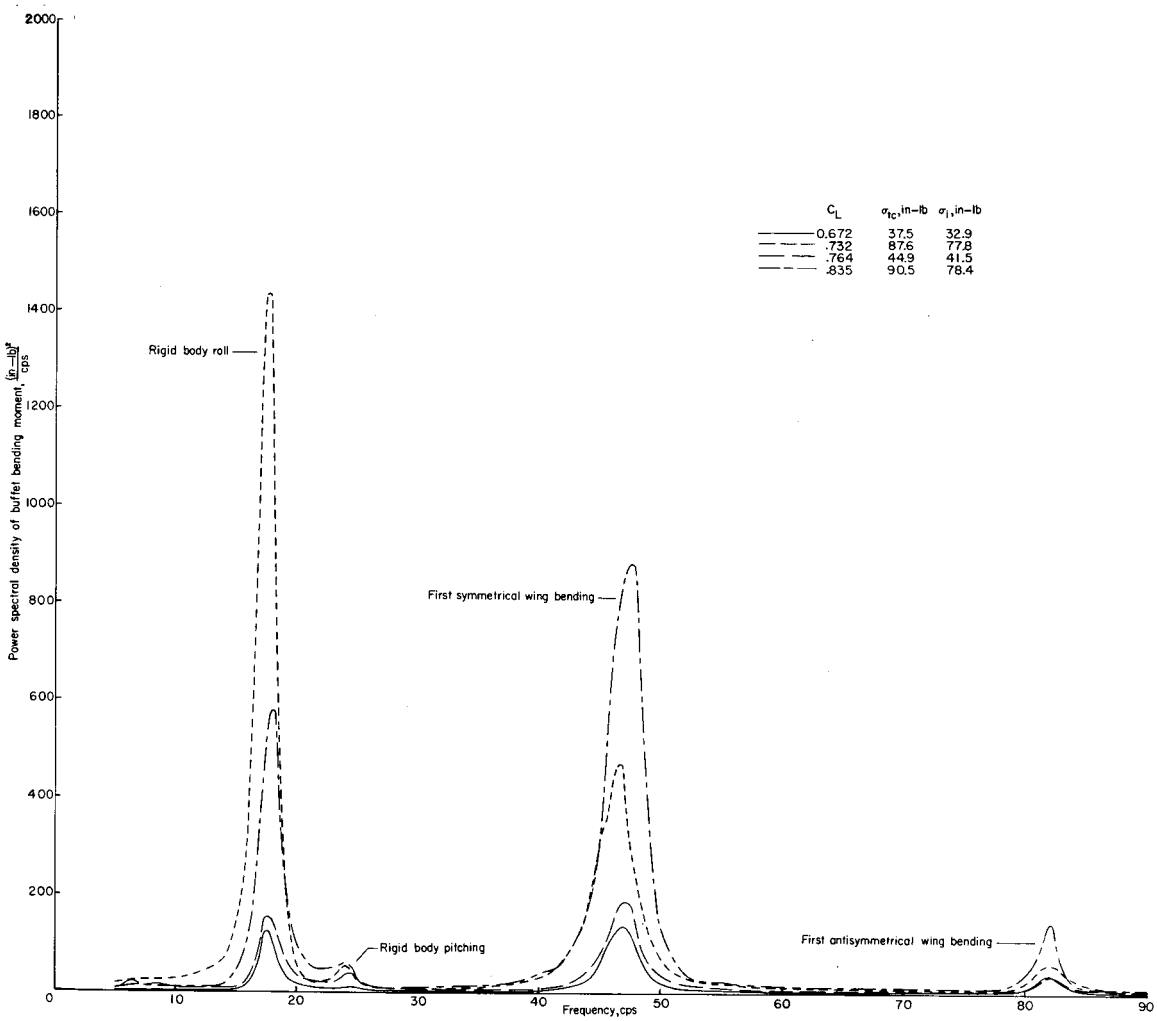

(d) M = 0.98; p_t = 0.4 atm.

Figure 15.- Continued.

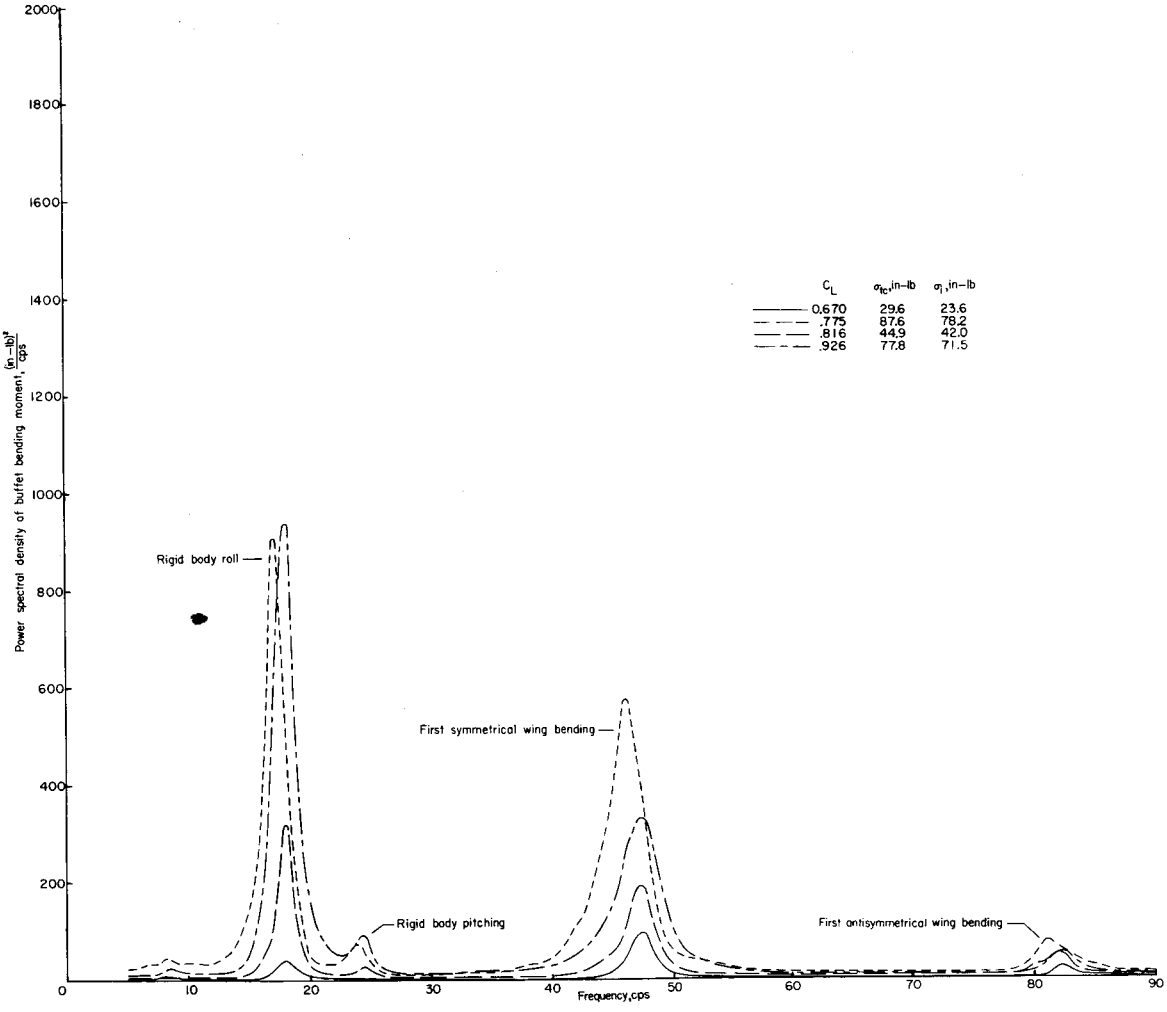

(e) M = 1.00; p_t = 0.4 atm.

Figure 15.- Continued.

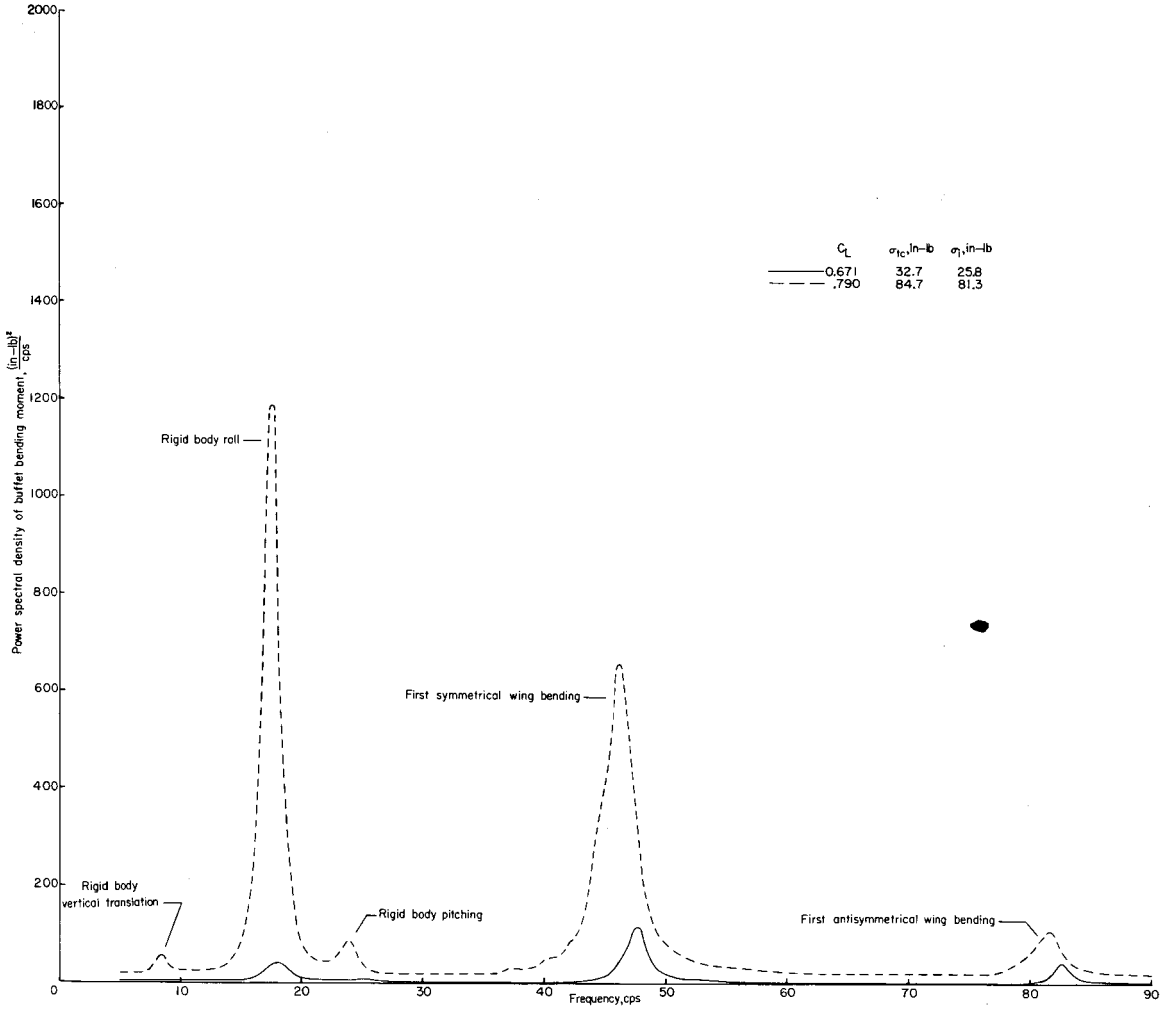

(f) M = 1.03; p_t = 0.4 atm.

Figure 15.- Concluded.

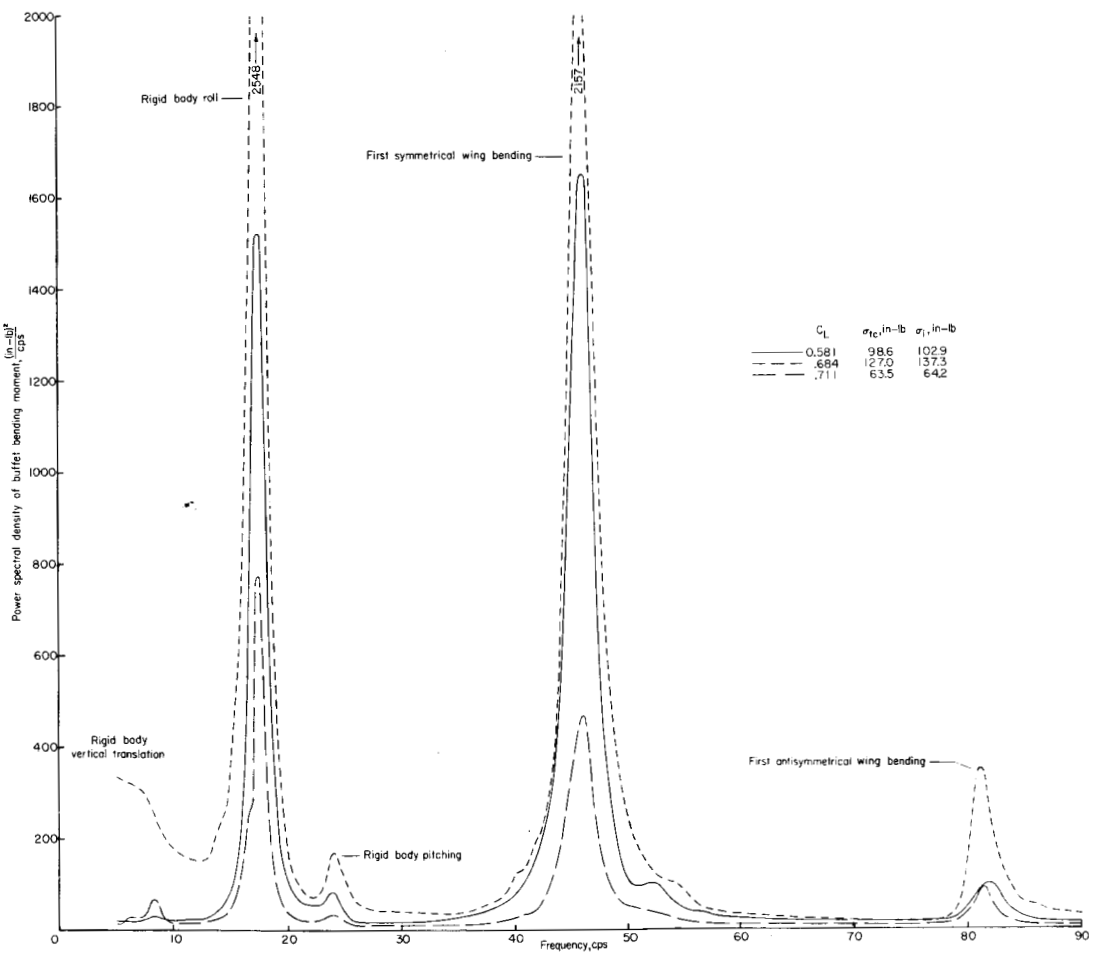

(a) M = 0.90; p_t = 0.4 atm.

Figure 16.- Power spectral density of buffet response at various test conditions for configuration 2 (W + F + FA + VT + HT). (Effective bandwidth of scanning bandpass filter was approximately 1.5 cps.)

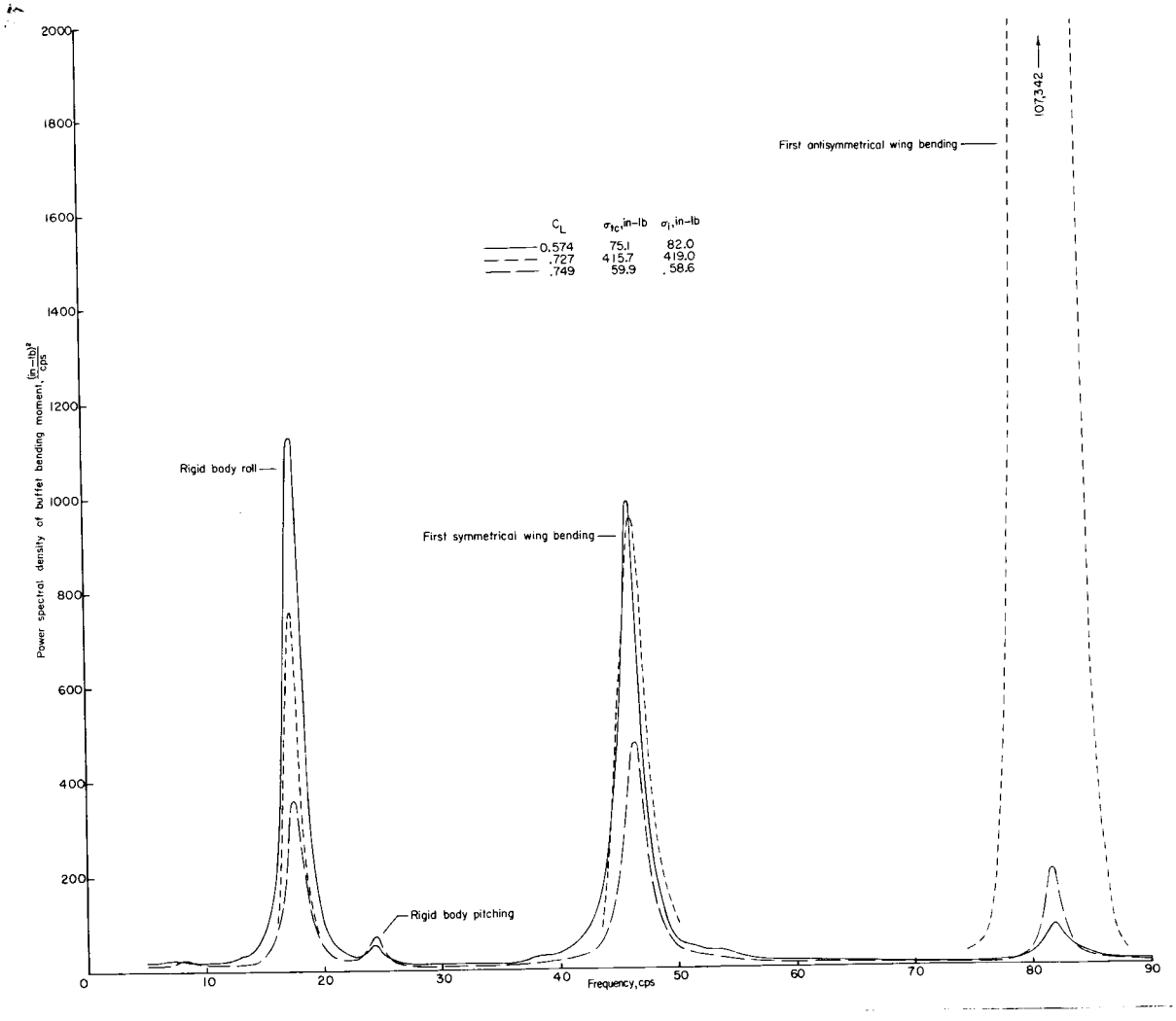

(b) M = 0.93; p_t = 0.4 atm.

Figure 16.- Continued.

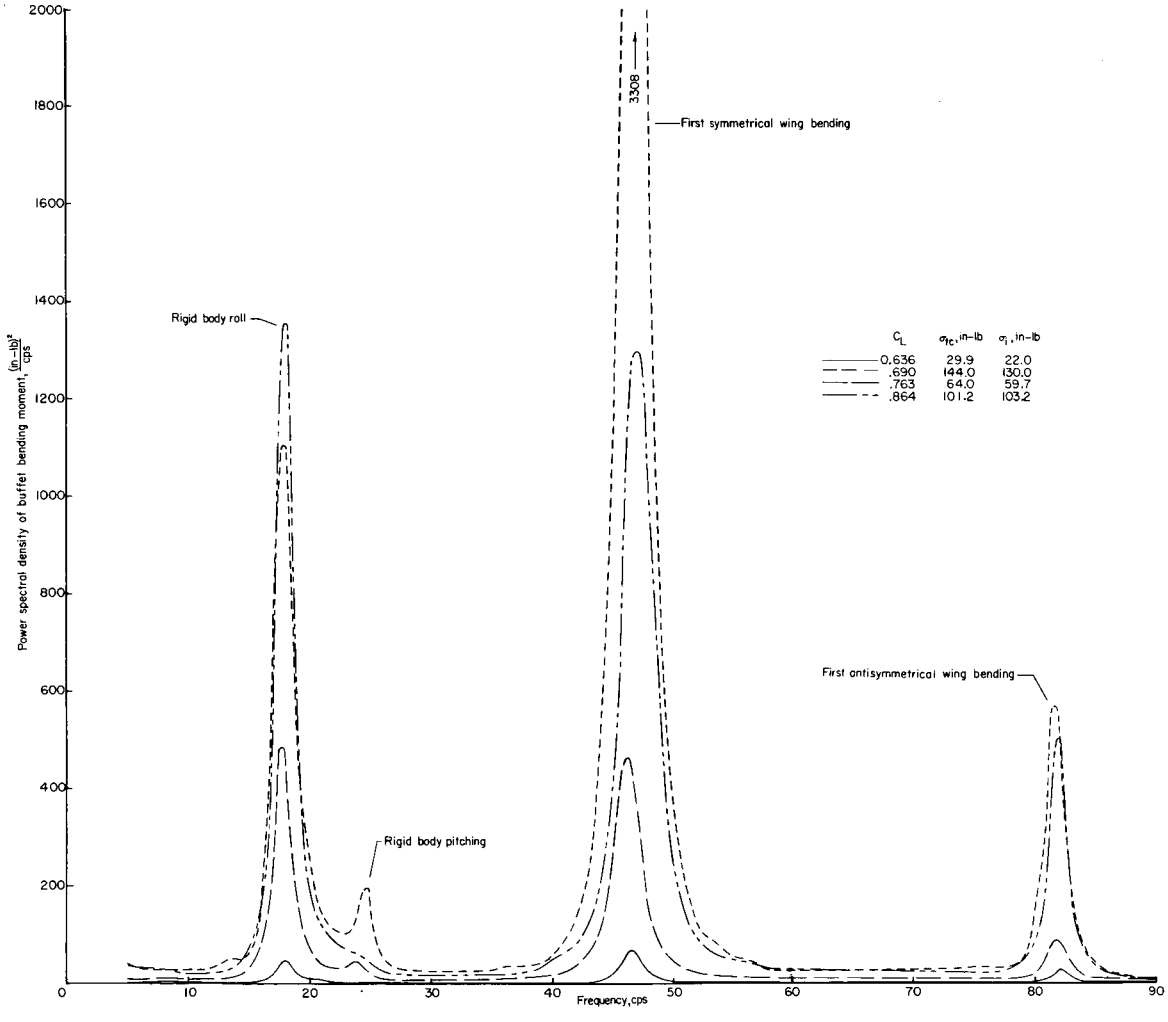

(c) M = 0.98; p_t = 0.4 atm.

Figure 16.- Concluded.

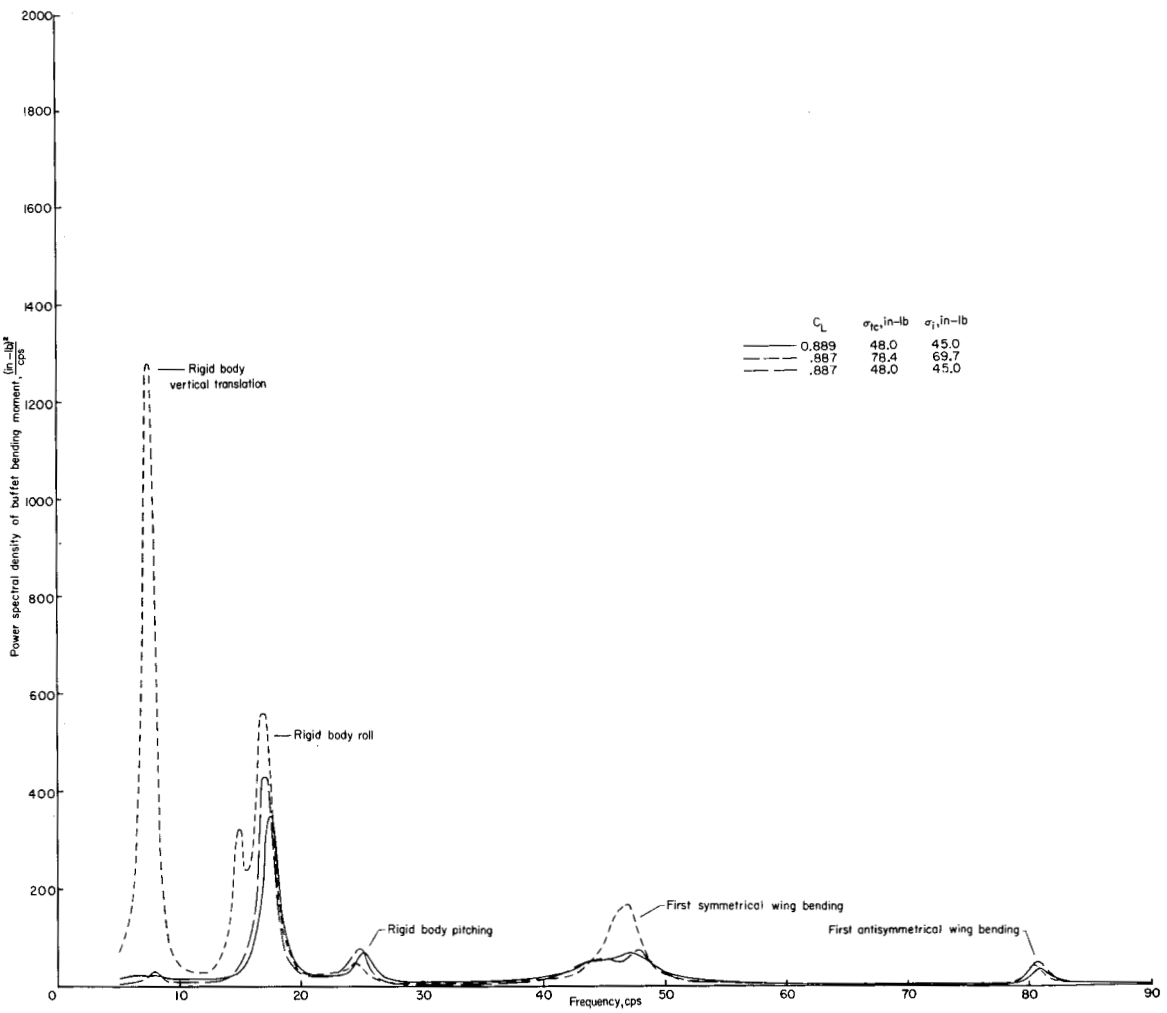

Figure 17.- Power spectral density of buffet response for configuration 3 (W + WB (1, 2, 3) + F + FA + VT + HT). M = 0.93; p_t = 0.4 atm. (Effective bandwidth of scanning bandpass filter was approximately 1.5 cps.)

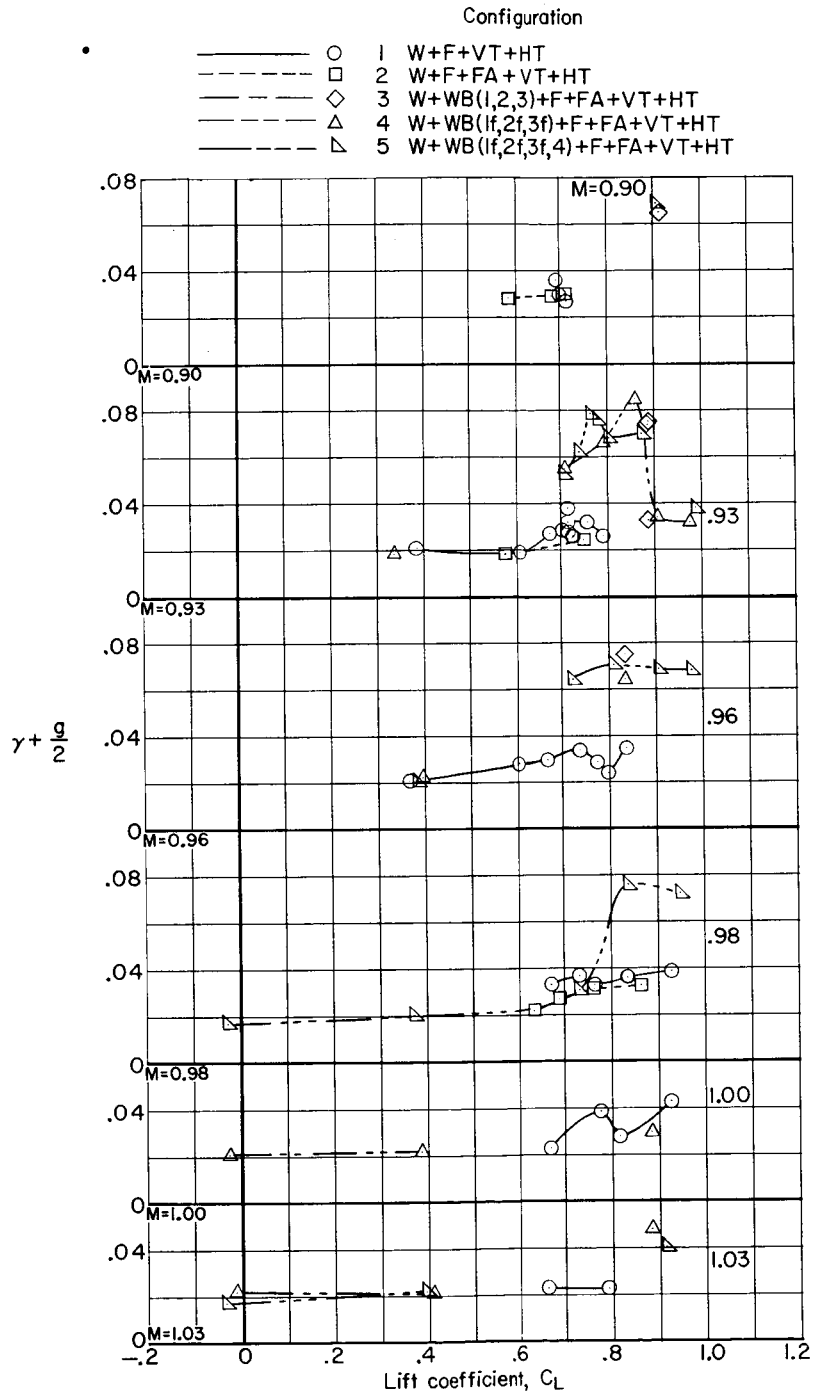

Figure 18.- Variation of total damping coefficient with lift coefficient for configurations 1 to 5. p_t = 0.4 atm.

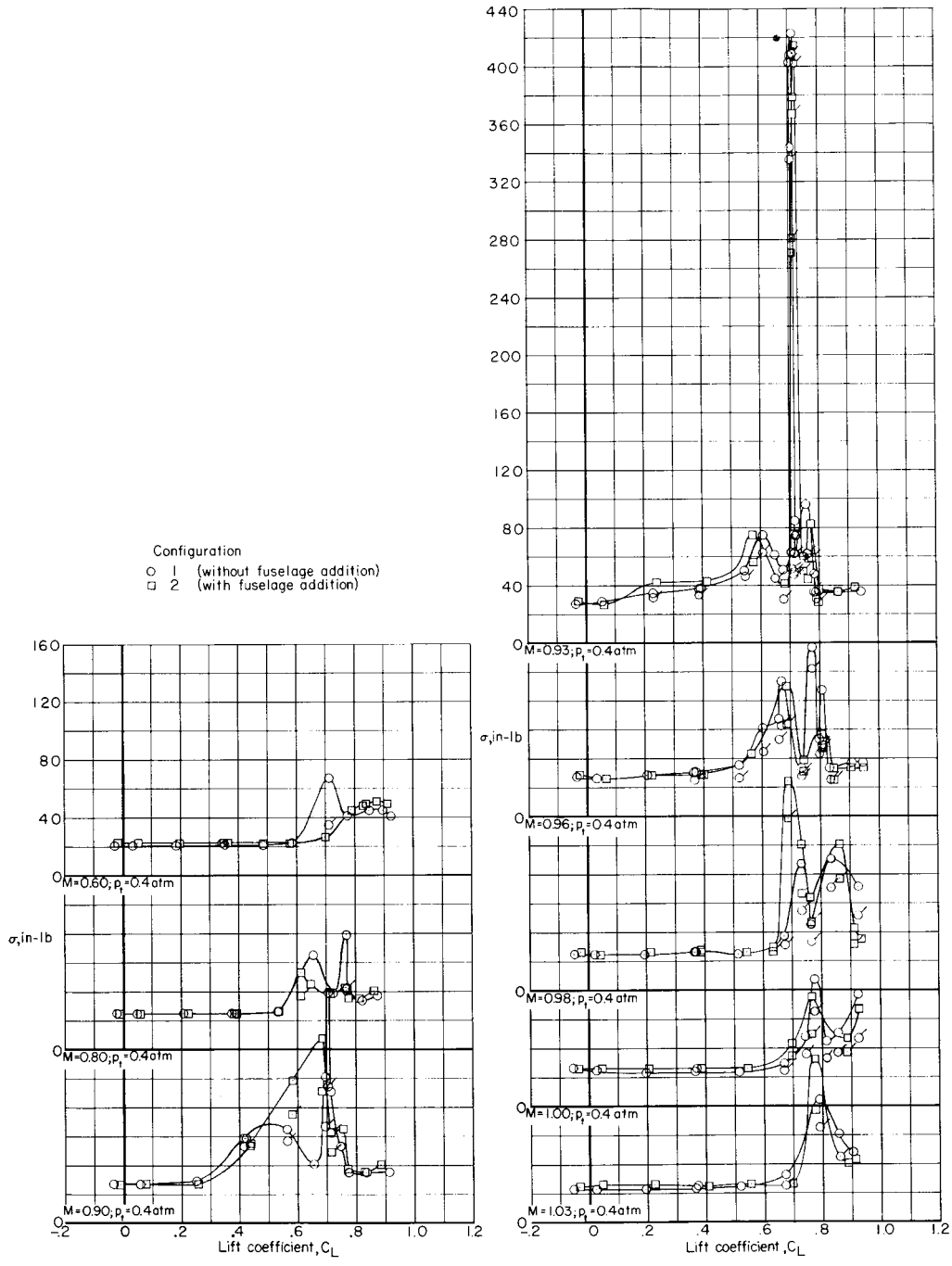

Figure 19.- Effect of fuselage addition upon the root-mean-square wing bending-moment fluctuations obtained from thermocouple-meter readings. (Flagged symbols indicate that the contribution of the model-support system has been filtered out.)

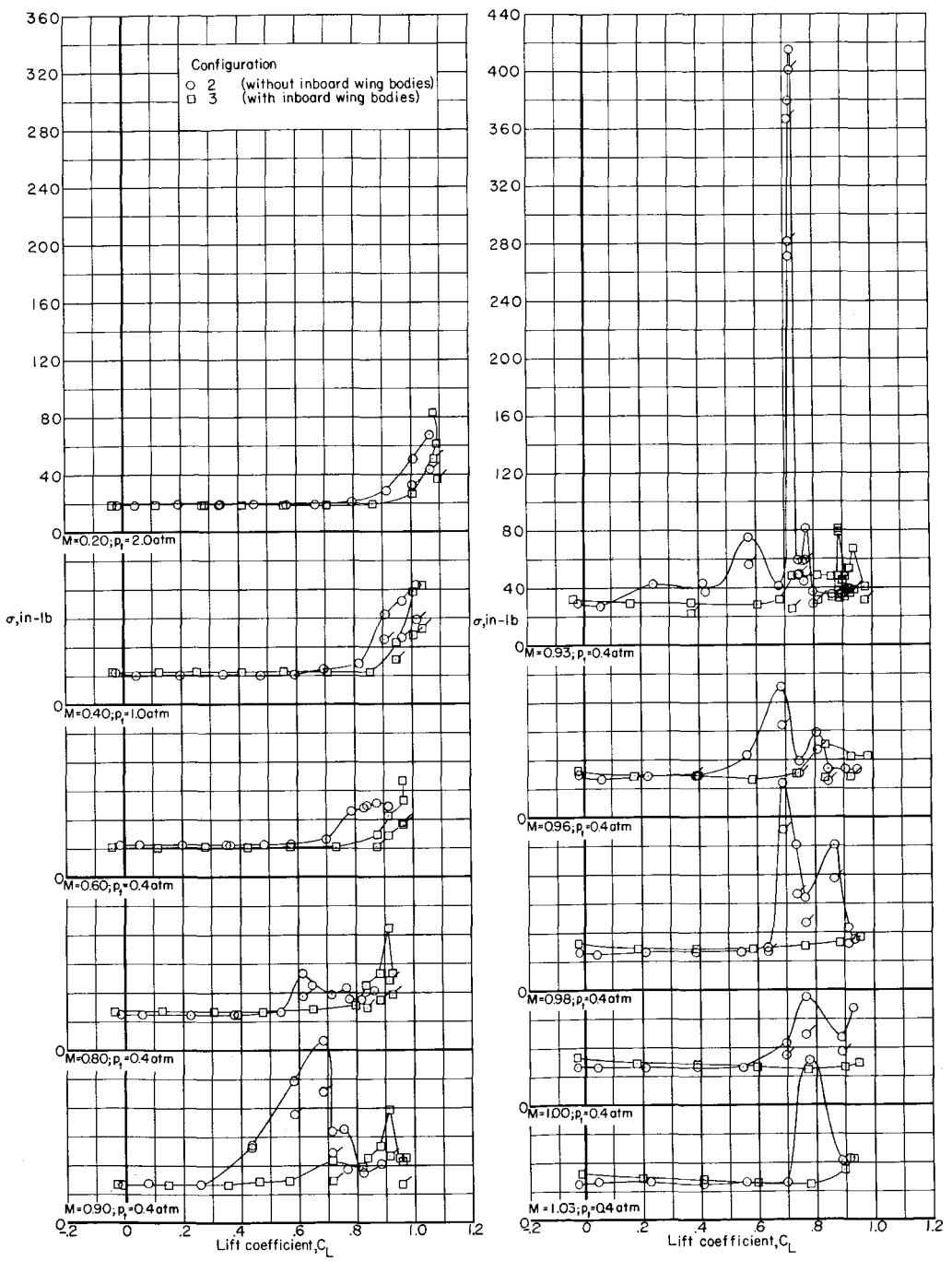

Figure 20.- Effect of three inboard wing bodies upon the root-mean-square wing bending-moment fluctuations obtained from thermocouple-meter readings. (Flagged symbols indicate that the contribution of the model-support system has been filtered out.)

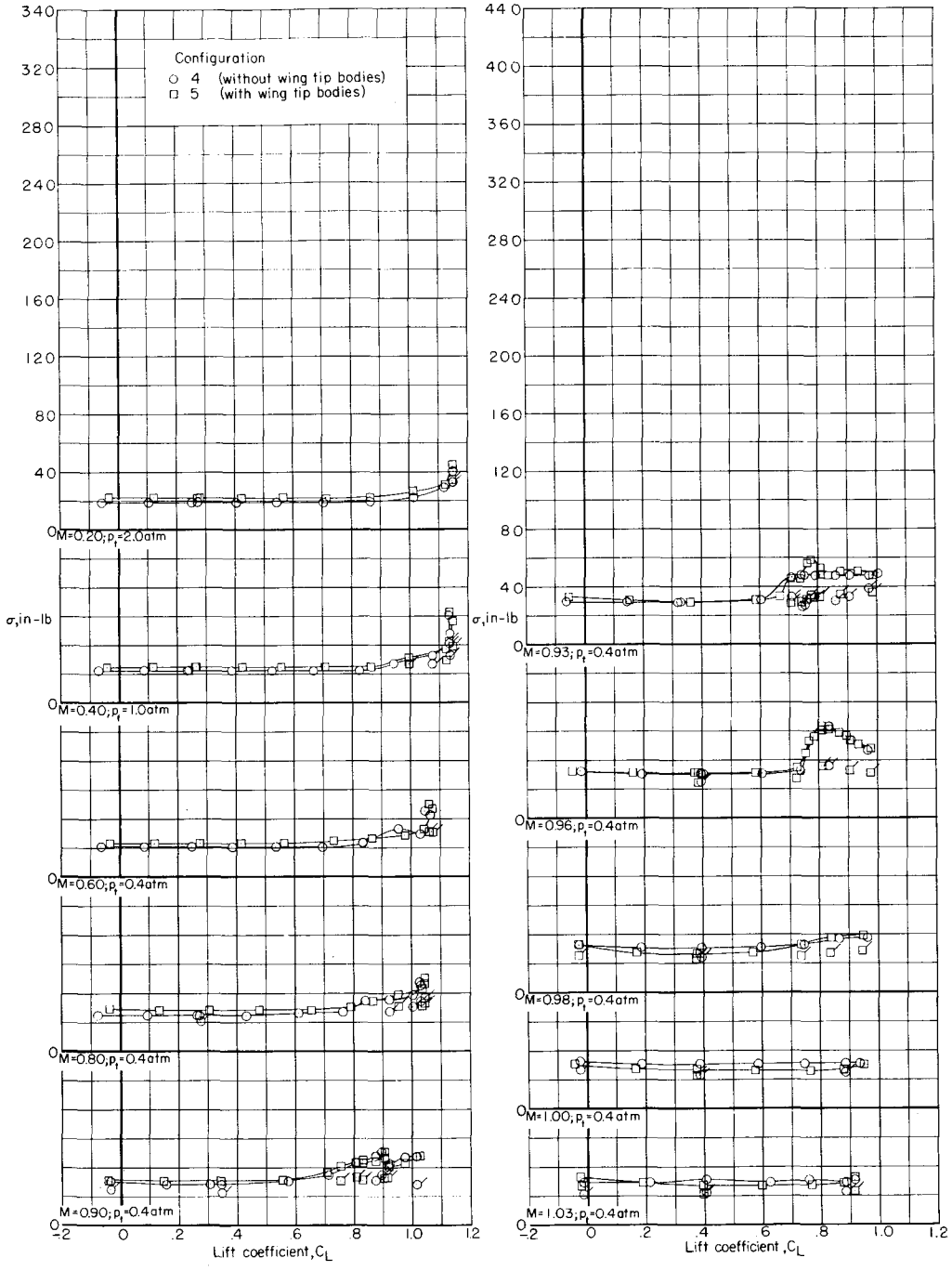

Figure 21.- Effect of wing-tip bodies upon the root-mean-square wing bending-moment fluctuations obtained from thermocouple-meter readings. (Flagged symbols indicate that the contribution of the model-support system has been filtered out.)

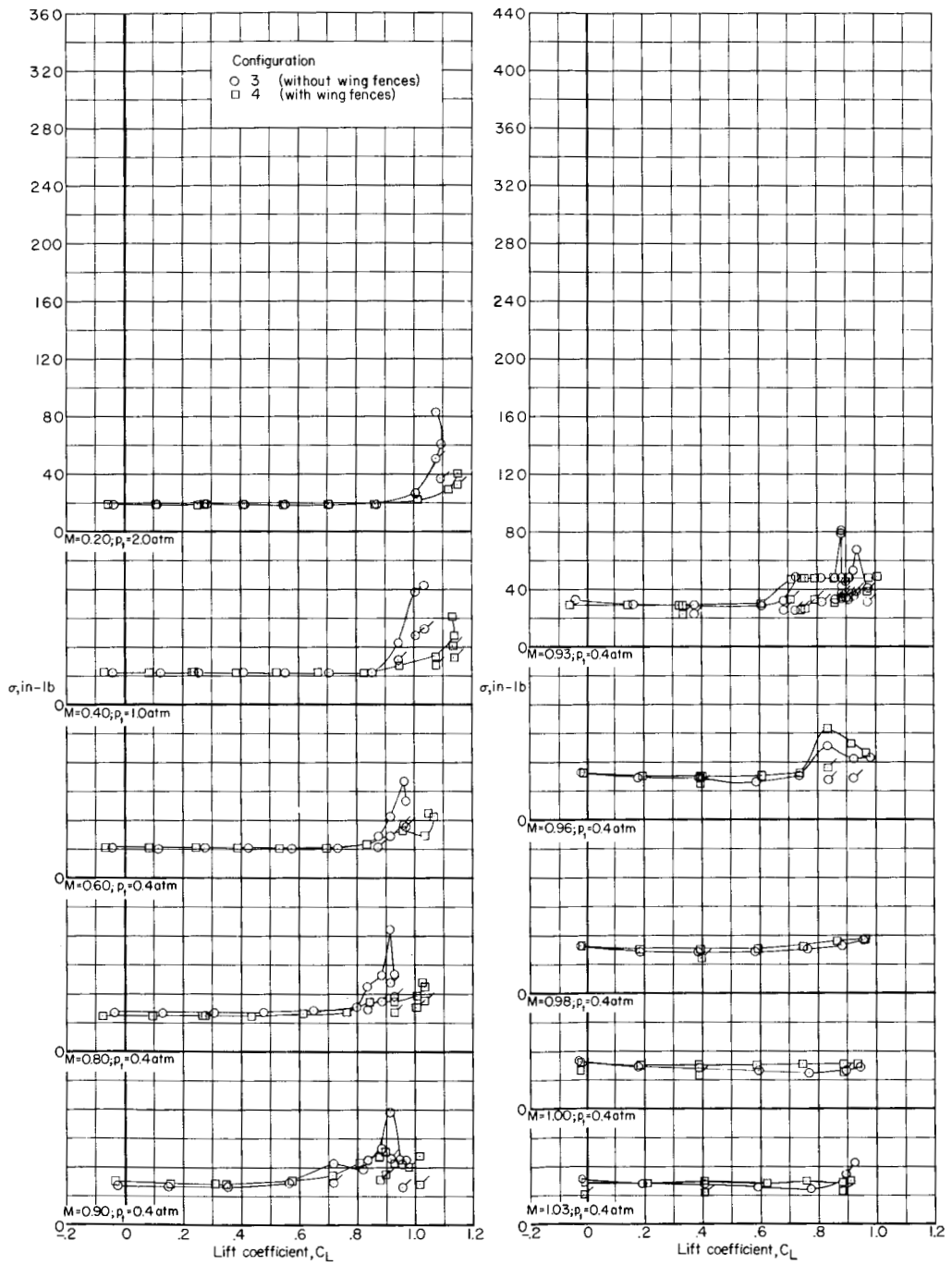

Figure 22.- Effect of wing fences upon the root-mean-square wing bending-moment fluctuations obtained from thermocouple-meter readings. (Flagged symbols indicate that the contribution of the model-support system has been filtered out.)

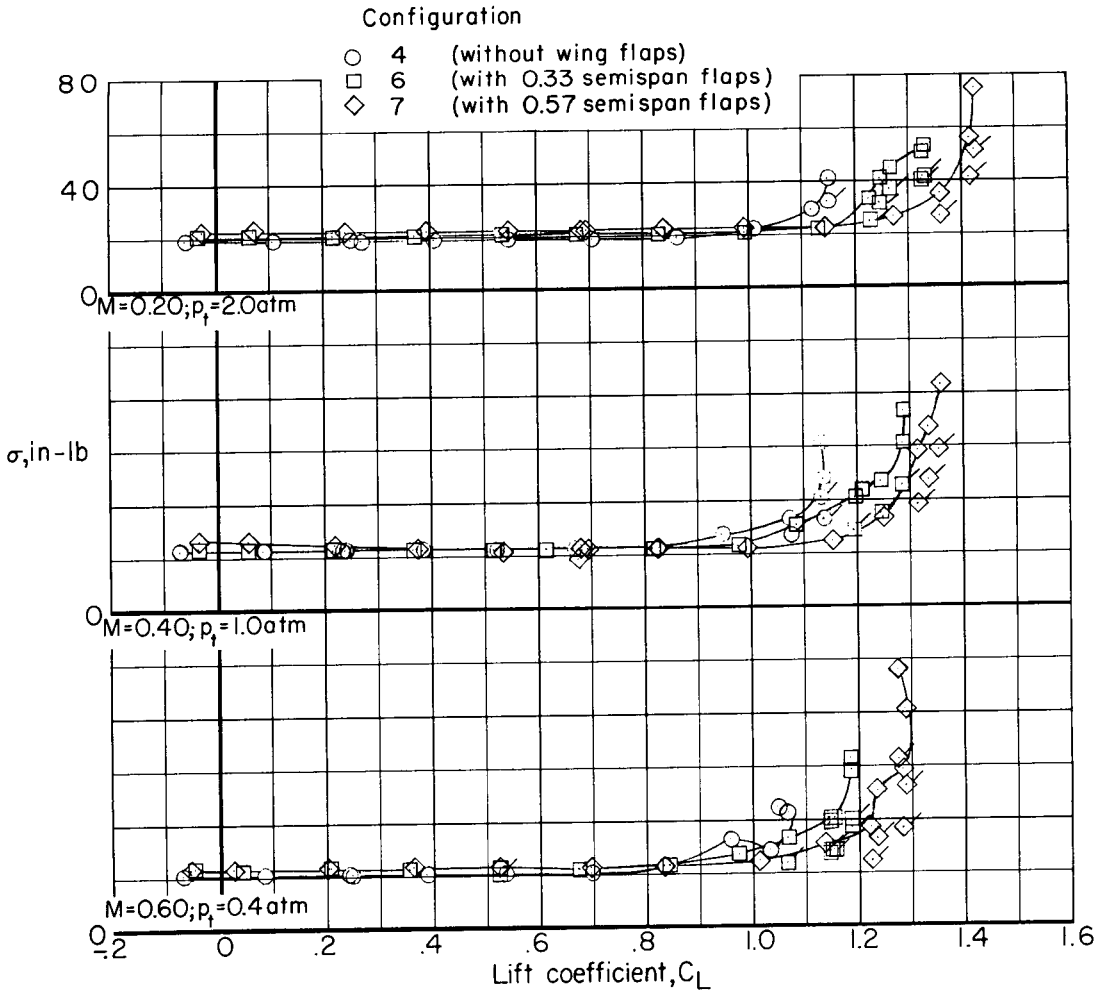

Figure 23.- Effect of wing flaps upon the root-mean-square wing bending-moment fluctuations obtained from thermocouple-meter readings. (Flagged symbols indicate that the contribution of the model-support system has been filtered out.)

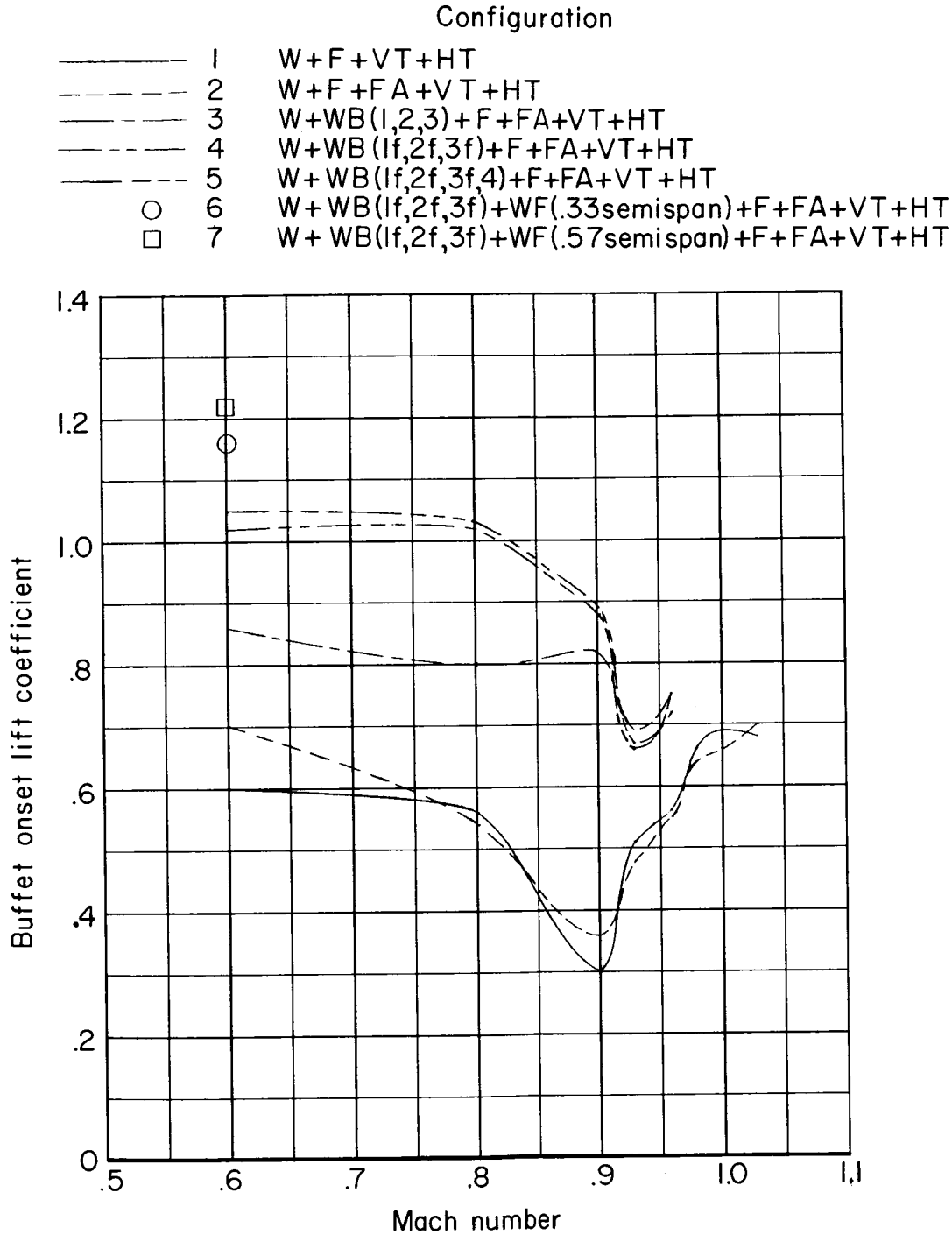

Figure 24.- Buffet onset boundaries for the various configurations. (p_t = 0.4 atm.)

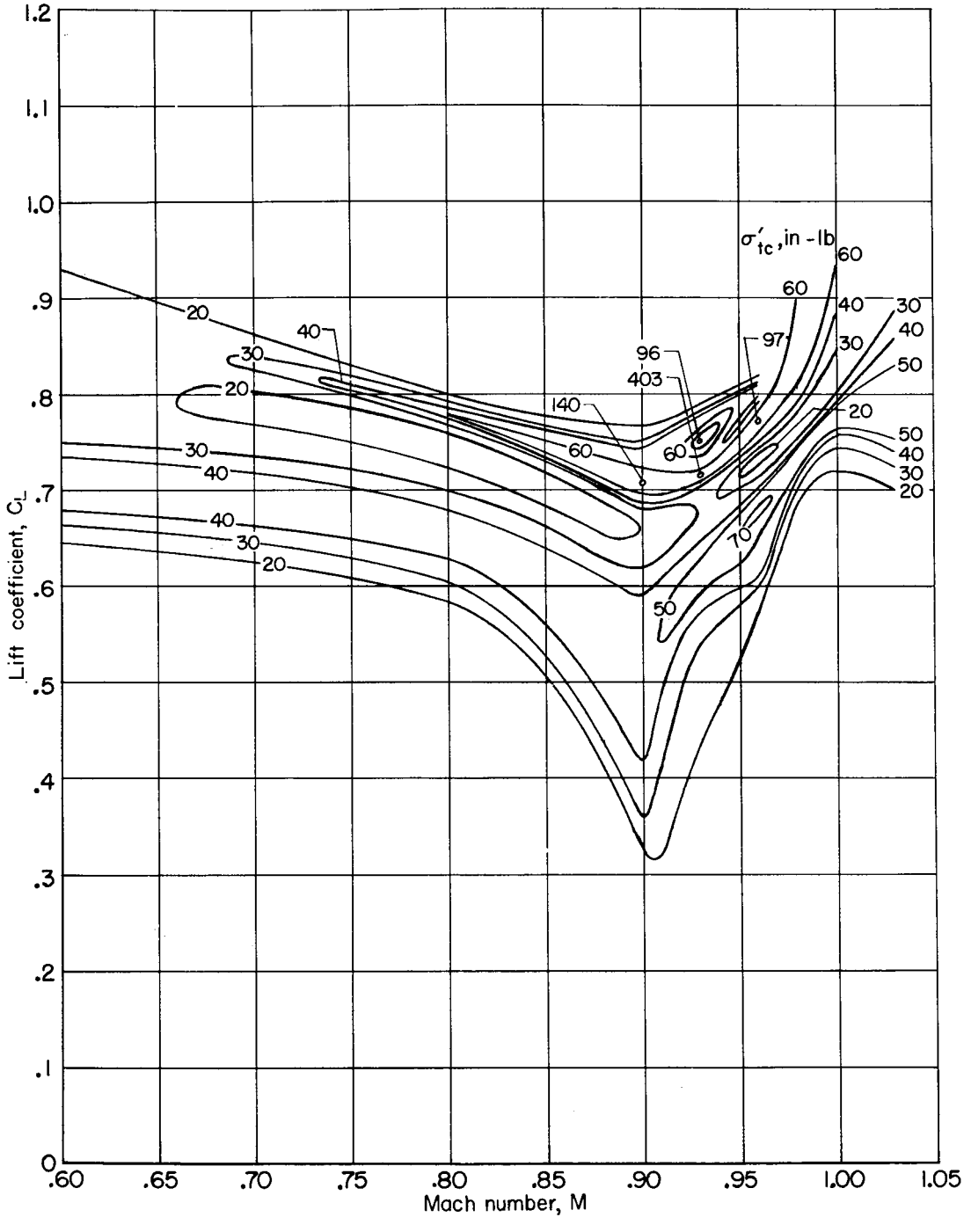

(a) Configuration 1 (W + F + VT + HT).

Figure 25.- Variation with Mach number of boundaries for constant buffet intensities for various configurations.

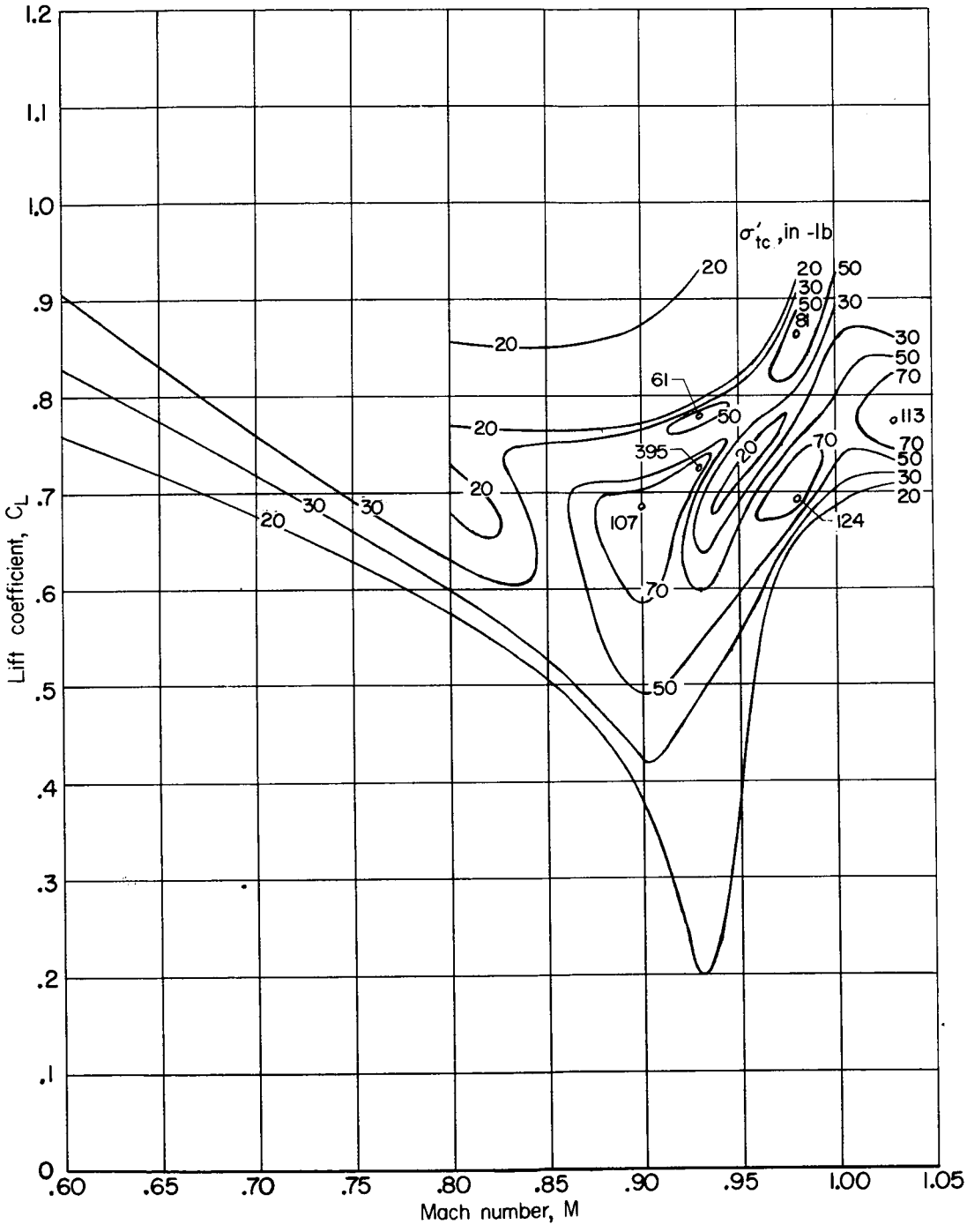

(b) Configuration 2 (W + F + FA + VT + HT).

Figure 25.- Continued.

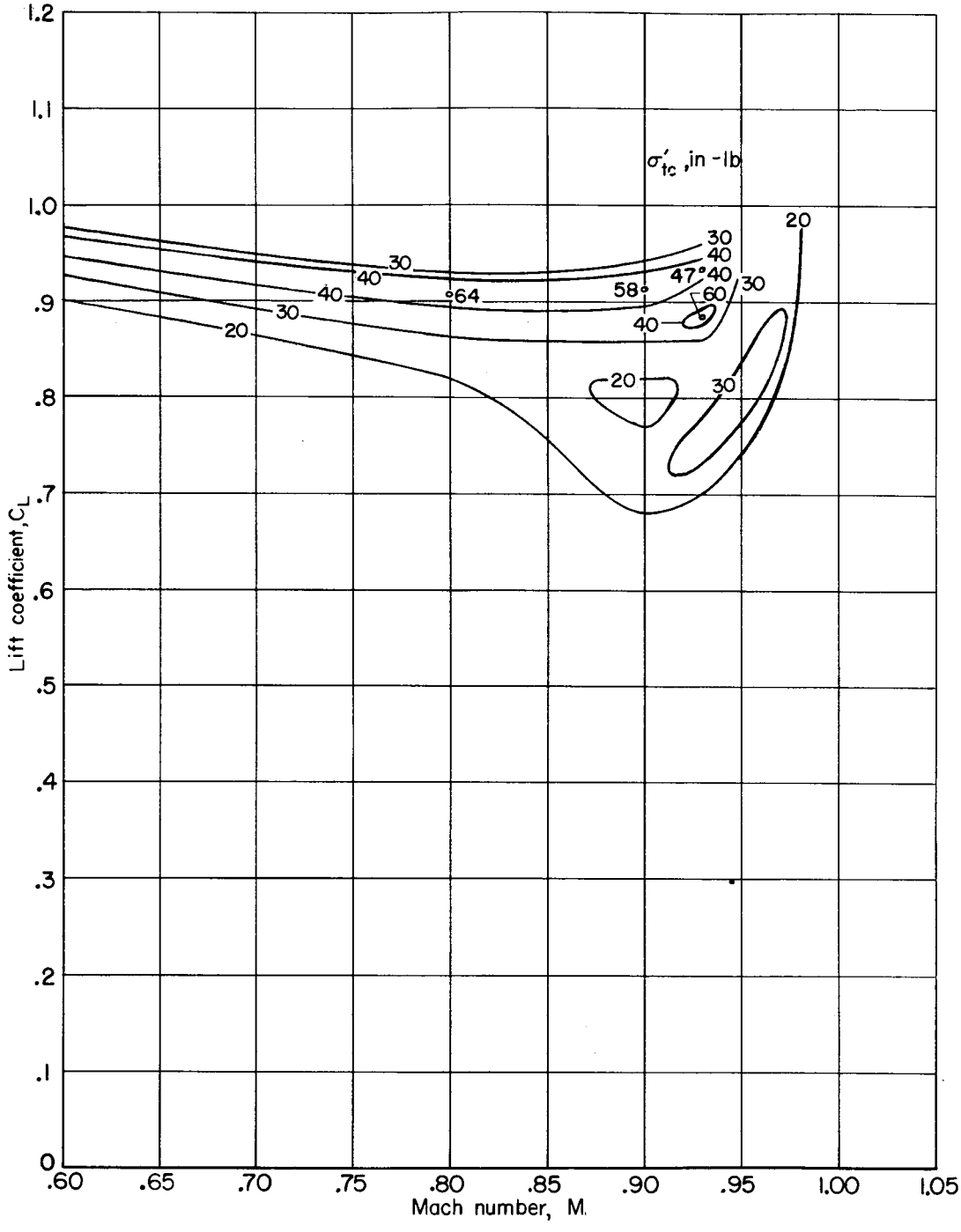

(c) Configuration 3 (W + WB(1, 2, 3) + F + FA + VT + HT).

Figure 25.- Continued.

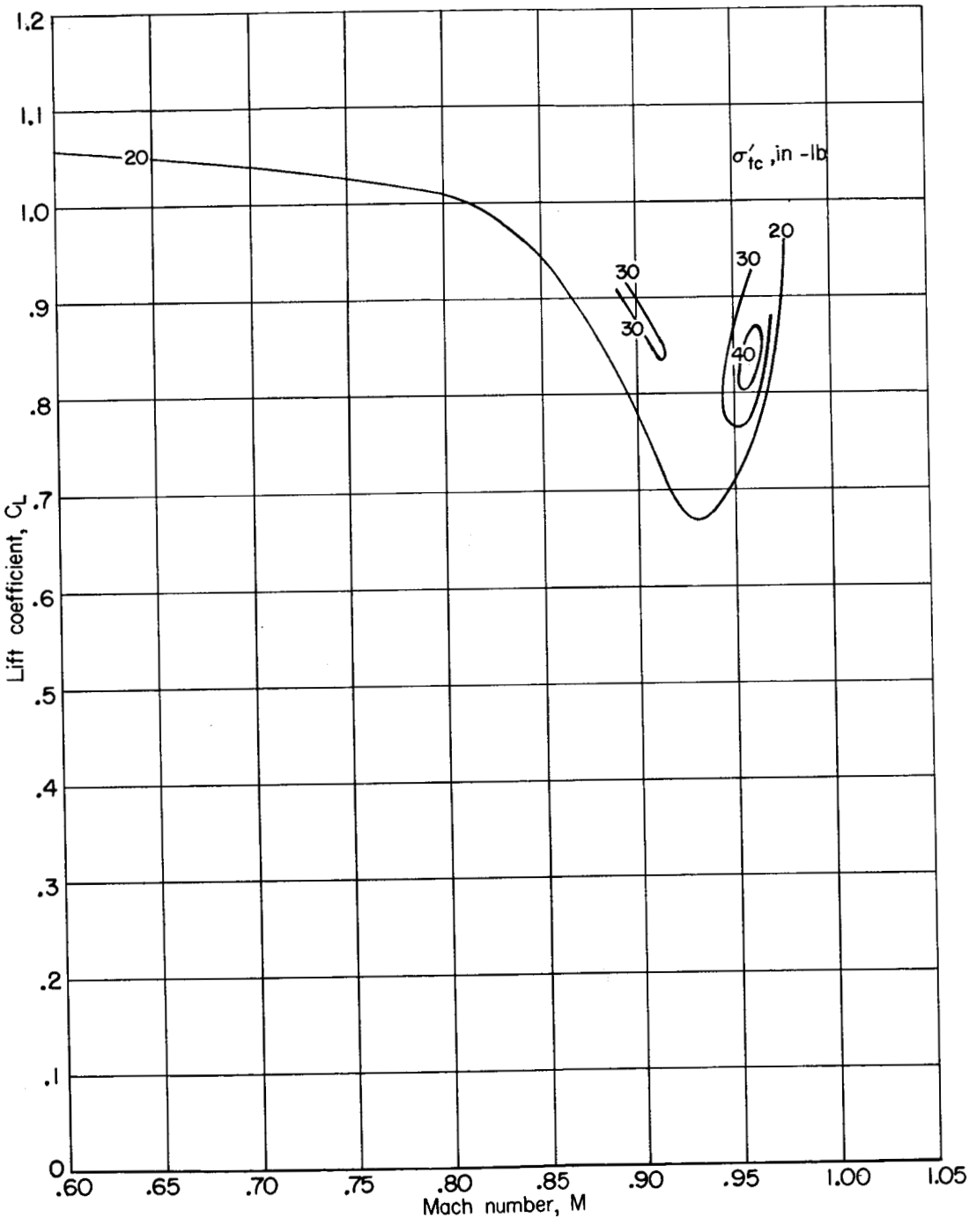

(d) Configuration 4 (W + WB(1f, 2f, 3f) + F + FA + VT + HT).

Figure 25.- Continued.

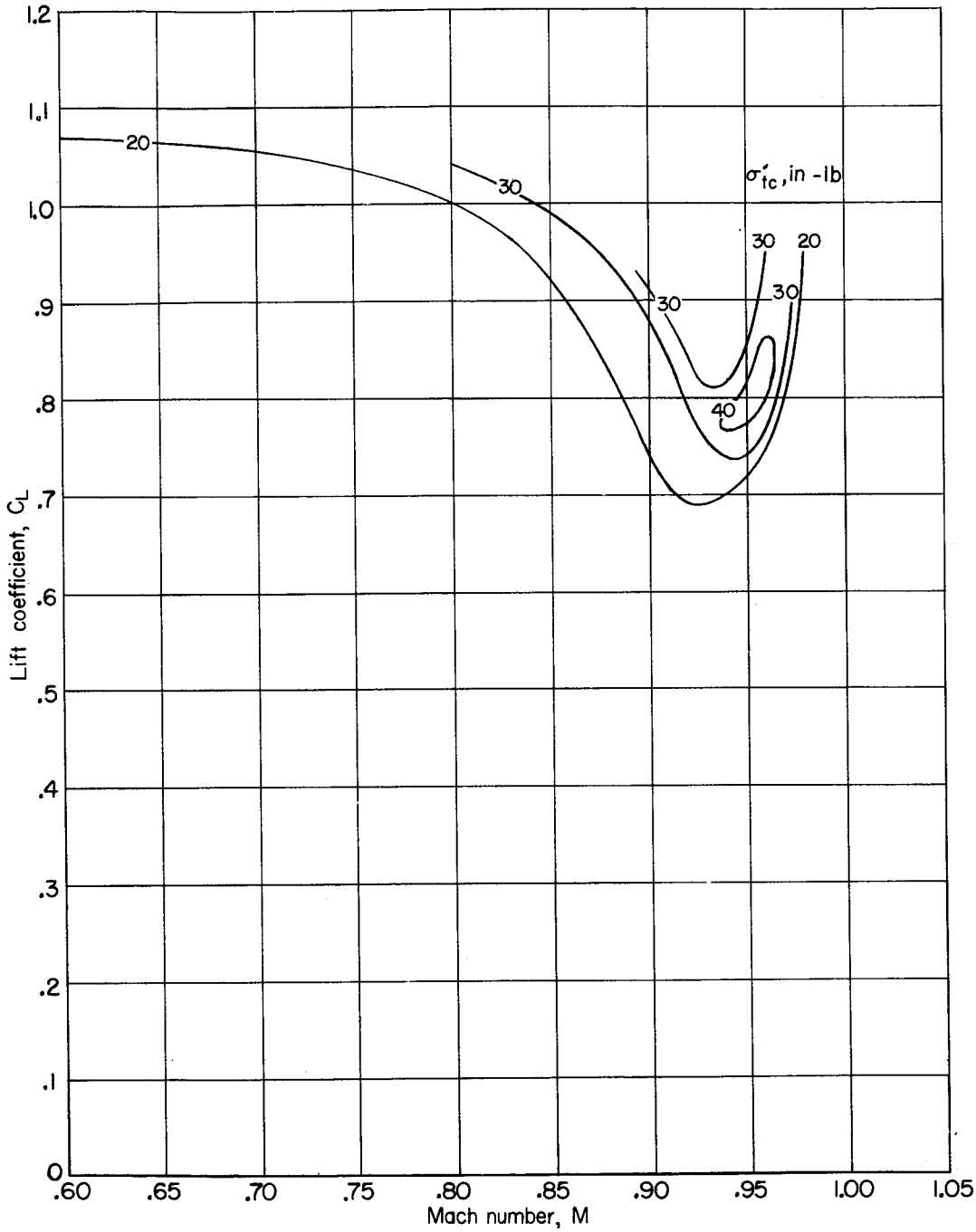

(e) Configuration 5 (W + WB(1f, 2f, 3f, 4) + F + FA + VT + HT).

Figure 25.- Concluded.

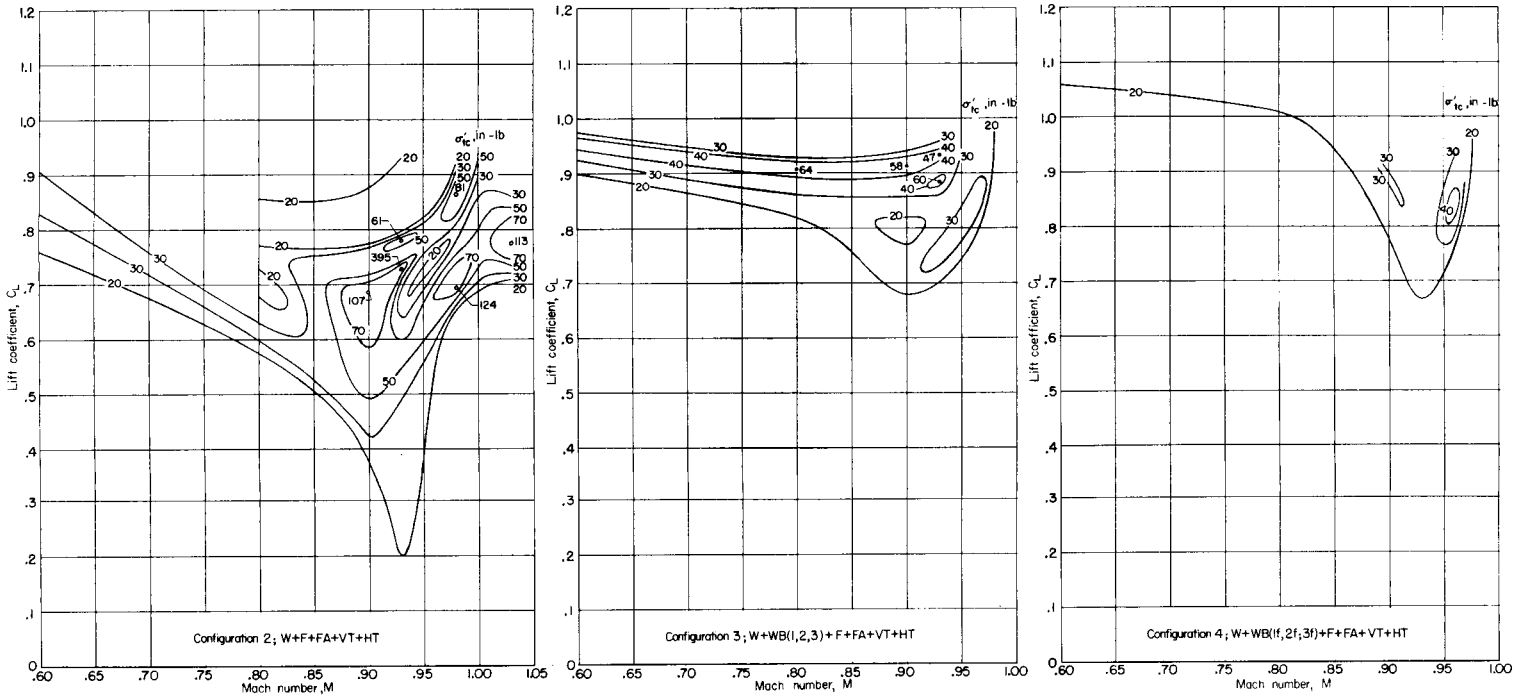

Figure 26.- Effect of adding inboard wing bodies and wing fences on the contours of constant buffet intensity.